

Received: 3 September 2021

Revised: 22 November 2021

Accepted: 24 November 2021

# A review of the rational interfacial designs and characterizations for solid-state lithium/sulfur cells

Youngwoo Choo<sup>1</sup>  | Yoon Hwa<sup>2</sup>  | Elton J. Cairns<sup>3,4</sup> 

<sup>1</sup> The School of Civil and Environmental Engineering, University of Technology Sydney, Ultimo, New South Wales, Australia

<sup>2</sup> School of Electrical, Computer and Energy Engineering, Arizona State University, Tempe, Arizona, USA

<sup>3</sup> Department of Chemical and Biomolecular Engineering, University of California, Berkeley, California, USA

<sup>4</sup> Energy Storage and Distributed Resources Division, Lawrence Berkeley National Laboratory, Berkeley, California, USA

## Correspondence

Prof. Y. Hwa, School of Electrical, Computer and Energy Engineering, Arizona State University, Tempe, AZ 85287, USA  
 Email: [yoon.hwa@asu.edu](mailto:yoon.hwa@asu.edu)

Elton J. Cairns, Prof. E. J. Cairns, Department of Chemical and Biomolecular Engineering, University of California, Berkeley, CA 94720, USA

Email: [ejcairns@lbl.gov](mailto:ejcairns@lbl.gov)

## Funding information

2021 Fulton Schools of Engineering Strategic Interest Seed Funding of Arizona State University

## Abstract

The high theoretical specific energy of lithium/sulfur (Li/S) cells (2600 Wh/kg) has positioned the Li/S cell as one of the most promising candidates for the beyond lithium-ion cell. Despite the evident advantages, there are remaining problems mainly associated with the unique solution-based reaction chemistry involving lithium polysulfide (Li-PS) that hinder the commercialization of the Li/S cells. Incorporating solid-state electrolytes (SSEs) can avoid the Li-PS shuttle problem while preserving the benefits of Li/S cells, but it introduces other challenges related to the electrode/electrolyte solid interfaces. This topical review summarizes the current status of solid-state Li/S cells and their major challenges and discusses the recent efforts to improve cell performance and durability. Various solid-state electrolytes, including oxides, sulfides, and solid polymer electrolytes, are briefly reviewed. In particular, we focus on the recent progress to improve the interfacial properties by two major approaches, morphological and chemical modifications of the electrode/electrolyte interfaces. The design strategy and implementation to overcome the prominent issues associated with sulfur electrodes are critically discussed. Also, several electrochemical and physicochemical characterization methods to examine the electron/ion transport at the interface are outlined. Given the superior theoretical physicochemical properties of the Li/S cells, we emphasize that the inappropriate interfacial design of the solid-state Li/S cells is the major challenge to bring solid-state Li/S cells to a commercially attractive level.

## KEYWORDS

characterization, interfaces, lithium/sulfur cells, solid electrolytes, solid-state battery

## 1 | INTRODUCTION

Currently, electrification of transportation systems is the ultimate goal to lower global greenhouse gas emissions that significantly contribute to climate change. Electric vehicle (EV) technology is an ideal solution to mitigate

the environmental crisis, and it is becoming more influential as the portion of electricity generation by clean, renewable energy sources increases. Significant technological progress has been made in passenger car technologies, and light-duty EVs reported excellent energy efficiency of up to 130 miles per gallon of gasoline equivalent (MPGe).<sup>[1]</sup>

This is an open access article under the terms of the [Creative Commons Attribution](https://creativecommons.org/licenses/by/4.0/) License, which permits use, distribution and reproduction in any medium, provided the original work is properly cited.

© 2021 The Authors. *Electrochemical Science Advances* published by Wiley-VCH GmbH.

However, we still need a significant breakthrough in battery technology to enable medium- and heavy-duty transportation such as trucks, buses, and trains that have a substantial contribution to the reduction of carbon emissions. Lithium-ion (Li-ion) cell technologies are a crucial enabler of electrified transportation, and their energy storage capability has still been improved. However, projected battery demand for larger applications indicates the need for enhanced energy storage capability and improved safety characteristics beyond the practical limit of current state-of-the-art lithium-ion cells.<sup>[2]</sup>

Solid-state lithium/sulfur (Li/S) cell technology has recently attracted attention as a next-generation rechargeable battery technology because of its high theoretical specific energy (2600 Wh/kg vs ~550 Wh/kg of conventional Li-ion cells consisting of graphite anode and lithium cobalt oxide cathode) and improved safety.<sup>[3–4]</sup> The high specific energy of solid-state Li/S cells is attributed to the high specific capacity of lithium metal and sulfur electrodes. Sulfur serving as an active material for the positive electrode is highly abundant and inexpensive, incredibly beneficial for large-scale battery production. On a practical level, the calculation of gravimetric energy density requires comprehensive considerations on the electrolyte layer thickness and sulfur loading in the positive electrodes. While a body of research efforts are underway to realize a practical Li/S pouch cell, the gravimetric energy density of a hypothetical Li/S cell is predicted to exceed 650 Wh/kg that is still a promising value compared to that of the commercial Li-ion cell.<sup>[5]</sup> In addition, the volumetric energy density of Li/S cells, which is another critical requirement for practical cell, is often limited because of the high electrolyte to sulfur (E/S) ratio and high porosity of a sulfur electrode.<sup>[6,7]</sup> While the limitation of a sulfur electrode is preserved in solid-state Li/S cell, the solid-state electrolytes enable the employment of a lithium metal anode and consequently enhance the volumetric energy density of the Li/S cells. In solid-state Li/S cells, a non-flammable solid superionic conductor with a wide temperature window is used instead of a flammable liquid organic electrolyte, which dramatically reduces any fire hazard and improves the reliability of battery cells in a wider range of operating temperatures. Moreover, solid electrolytes for Li/S cells are an ideal solution for the problematic lithium polysulfide (Li-PS) shuttle phenomenon that is one of the main reasons for the performance degradation of conventional Li/S cells. During the electrochemical process of a sulfur electrode in conventional Li/S cells, the lithium-sulfur intermediates, Li-PS (a series of binary intermediates referred to as  $\text{Li}_2\text{S}_x$  ( $1 < x \leq 8$ )), are formed at the sulfur/liquid electrolyte interface and dissolve into the liquid electrolyte. The Li-PS in the liquid electrolyte adjacent to the sulfur electrode migrate and dif-

fuse to the lithium electrode and are reduced at the surface of the lithium electrode, which leaves a deposit of  $\text{Li}_2\text{S}$  on the lithium electrode surface. Then, the Li-PS move back to the sulfur electrode and take sulfur from the sulfur electrode again. This continuous reaction loop driven by Li-PS is called the Li-PS shuttle phenomenon<sup>[8]</sup>. In principle, the Li-PS cannot exist in the solid-state, thus the solid-state Li/S cell that does not involve liquid electrolyte can be an ideal candidate for the prevention of the Li-PS shuttle effect.

The first thing that needs to be achieved is developing a superionic conductor with a conductivity comparable to that of organic liquid electrolytes. In this context, a number of works have been performed to explore solid-state electrolytes (SSEs) for Li/S cells, e.g., polymers, inorganic oxides, and sulfides.<sup>[9–19]</sup> Inorganic oxide SSEs including NASICON-type SSEs (e.g.,  $\text{Li}_{1+x}\text{Al}_x\text{Ti}_{2-x}(\text{PO}_4)_3$  (LATP),  $\text{Li}_{1+x}\text{Al}_x\text{Ge}_{2-x}(\text{PO}_4)_3$  (LAGP))<sup>[20–22]</sup>, garnet-type SSEs (e.g.,  $\text{Li}_2\text{La}_3\text{Zr}_2\text{O}_{12}$  (LLZO),  $\text{Li}_7\text{La}_{2.75}\text{Ca}_{0.25}\text{Zr}_{1.75}\text{Nb}_{0.25}\text{O}_{12}$  (LLCZN)),<sup>[23–24]</sup> and perovskite-type SSEs (e.g.,  $\text{Li}_{3x}\text{La}_{(2/3)-x}\text{TiO}_3$  (LLTO))<sup>[25]</sup> have been intensively studied for Li/S solid-state cells because of the good ionic conductivity and chemical/electrochemical stability. The NASICON type electrolyte was reported by Goode-nough et al.<sup>[26]</sup> and generally has a chemical formula of  $\text{AM}_2(\text{PO}_4)_3$ , where A is Li, Na, or K, and M is Ge, Zr, or Ti. Aluminum doping to the M site is often performed to improve the ionic conductivity of the solid electrolyte. The NASICON-type SSEs (e.g., LATP and LAGP) typically exhibit a good ionic conductivity of up to  $\sim 10^{-3}$  S/cm at room temperature and chemical, mechanical, and thermal stability<sup>[27]</sup>. The relatively low cost of raw material has made the NASICON-type SSE a feasible candidate for an SSE. Garnet-type electrolytes generally have the chemical formula of  $\text{A}_3\text{B}_2\text{C}_3\text{O}_{12}$ . High valence doping of metals, e.g., Te, Ta, Nb, Sb, and Sr, enhances the ionic conductivity and chemical stability in contact with lithium. Garnet-type SSEs such as LLZO and LLCZN also display excellent ionic conductivity ( $\sim 10^{-3}$  S/cm) and superior chemical stability with lithium metal. In addition, the garnet-type SSEs show a good electrochemical stability window and a wide voltage window.<sup>[28]</sup> Perovskite-type structures typically have a simple cubic symmetry with a chemical formula of  $\text{ABO}_3$ . A-site deficient perovskites are commonly used for the lithium-ion conductor, which permits the lithium-ion to move through the A-site vacancies.<sup>[29]</sup> Perovskite-type SSEs (LLTO) have good chemical and thermal stability, enhancing the cell's safety. Although oxide SSEs promise fast ion conduction and good chemical/electrochemical stability, due to the inferior interfacial contact originating from hard solid nature, the large interfacial impedance present at the electrode/electrolyte interface is a challenge that must be overcome.

Sulfide-based SSEs include glass-ceramic sulfides ( $x\text{Li}_2\text{S}(1-x)\text{P}_2\text{S}_5$  and  $x\text{Li}_2\text{S}(1-x)\text{SiS}_2$ ) and crystalline sulfides, for example, thio-LISICON ( $\text{Li}_{4-x}\text{Ge}_{1-x}\text{P}_x\text{S}_4$ ),  $\text{Li}_7\text{P}_3\text{S}_{11}$ ,  $\text{Li}_{10}\text{MP}_2\text{S}_{12}$  ( $M = \text{Ge}, \text{Sn}, \text{Si}$ ), argyrodite ( $\text{Li}_6\text{PS}_5\text{X}$  ( $X = \text{Cl}, \text{Br}$ )), and  $\text{LiSiPSCl}$ .<sup>[30]</sup> The sulfide solid electrolytes offer higher ionic conductivity at room temperature than conventional oxide-based solid electrolytes. High ionic conductivity of the sulfide solid electrolyte is mainly attributed to the lower electro-negativity and larger ionic radius of sulfur anions than oxygen anions, resulting in wider lithium-ion channels and easier dissociation of lithium-ions from the anion sublattice.<sup>[31]</sup> In addition, the sulfide solid electrolytes show low electronic conductivities ( $\approx \text{nS/cm}$ ), high lithium transference numbers ( $\approx 1$ ), and highly ductile properties, which are ideal properties for use in a solid-state battery.<sup>[32]</sup> Glass sulfides were initially studied, and the ratio of the  $\text{Li}_2\text{S}$  to  $\text{P}_2\text{S}_5$  was adjusted to find an optimized ionic conductivity ( $\sim 10^{-4}$  S/cm at  $25^\circ\text{C}$ ).<sup>[33]</sup> Crystalline sulfides demonstrate outstanding ionic conductivities of over  $10^{-2}$  S/cm at room temperature, comparable to the conductivity of conventional organic liquid electrolytes. In contrast to the oxide SSEs, sulfides typically show smaller grain boundary resistance. Sulfides also have a wide electrochemical window and appropriate mechanical properties such as formability and elastic modulus, reducing the interfacial resistance compared to oxide SSEs. Despite the great advantages and excellent electrochemical performance of sulfides, the high reactivity with moisture that leads to the generation of toxic  $\text{H}_2\text{S}$  and chemical/electrochemical instability with electrode materials hamper the utilization of the sulfides as SSEs.<sup>[34]</sup>

Besides the inorganic superionic conductors, solid polymer electrolytes (SPEs) have been investigated as SSEs in Li/S cells.<sup>[35–36]</sup> Polymer electrolytes are typically prepared by mixing lithium salts, e.g., lithium bis(fluorosulfonyl)imide (LiFSI), with poly(ethylene oxide) (PEO), polyvinylidene fluoride (PVDF), or polysiloxane-based polymers.<sup>[37–41]</sup> Oxygen atoms present in a polymer backbone provide coordination sites for lithium cations, and the ions move within the polymer matrices as dictated by the segmental motion of the polymer chains.<sup>[42]</sup> Polymer electrolytes have good chemical stability with many electrode materials and show excellent interfacial contact between the electrode and electrolyte due to the superior flexibility compared to other inorganic SSEs.<sup>[43–44]</sup> Furthermore, the preparation process is simple and cost-effective. However, the ionic conductivity of the polymer electrolytes at room temperature is lower than the organic liquid electrolyte counterpart or other inorganic SSEs. Gel polymer electrolytes (GPEs) are also actively studied in Li/S cells as a viable method

to enhance ionic conductivity.<sup>[45]</sup> However, the GPEs typically include liquid electrolytes, and thus, the issues related to the organic liquid electrolyte still exist in GPEs.

The remarkable advances in solid superionic conductors have attracted attention to the solid-state Li/S cells, but the excellent ionic conductivity of the solid electrolytes is often accompanied by the uncontrolled and unstable electrode/solid electrolyte interfaces that cause high interfacial impedance. In liquid electrolyte-based Li/S cells, a liquid electrolyte spontaneously forms continuous ion conduction pathways and an adequate electrode/electrolyte interface by filling the pores of electrodes and wetting the electrode surface. However, unlike the liquid electrolyte-based Li/S cells, various interfaces that hamper electron/ion transport from or to the electrodes negatively affect the electrochemical process of the solid-state Li/S cells. The lithium metal anode essential to achieve high specific energy has some technical problems that remain unsolved. The lithium anode-solid electrolyte interface generally has a relatively flat structure as lithium foil is preferentially used for solid-state Li/S cells. Intensive research on the lithium metal/solid electrolyte interface has revealed significant concerns:<sup>[46–50]</sup> (1) chemical instability of the solid electrolyte in contact with highly reactive lithium metal, which causes decomposition of the solid electrolyte and formation of an undesired solid electrolyte interphase (SEI); (2) inhomogeneous lithium stripping/plating behavior which can create localized stress applied to the solid electrolyte, resulting in uncontrolled lithium dendrite formation and penetration through the solid electrolyte. Previously, it was expected that the high mechanical strength of the solid electrolytes could prevent internal cell shorting caused by lithium dendrite growth. However, recent studies indicate that uncontrolled lithium dendrite growth could still be an issue for all-solid-state systems.<sup>[51]</sup>

In contrast to the lithium anode-solid electrolyte interface, the sulfur cathode-solid electrolyte interface is more complicated as most sulfur electrodes are composed of multiple solid constituents such as active sulfur, carbon additives, and a polymer (binder). The microstructure of the sulfur electrode prepared by the slurry-based tape casting method is very random and porous. In sulfur electrodes, the electronic conduction path is established by interparticle contact of carbon additives, but the ionic percolation network forms differently for conventional Li/S cells and solid-state Li/S cells. In a conventional Li/S cell that uses liquid electrolytes, an ion percolation network is established by a liquid electrolyte that spontaneously fills the pores of the sulfur electrode once incorporated into the Li/S cell. However, the ionic percolation network of the sulfur electrode in solid-state Li/S cells relies on the interparticle contact of the solid electrolyte, so the interparticle

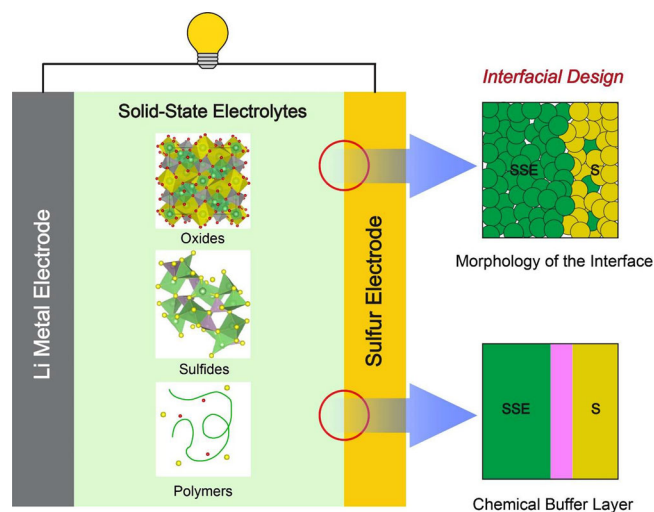


**FIGURE 1** Schematic illustration of the solid-state Li/S cell

network must be continuous and have an adequate interface with sulfur particles for a sufficient supply of lithium-ions to the active sulfur.

Consequently, each carbon (electronic conduction path) and solid electrolyte (ionic conduction path) have to form an individual continuous network, but both should provide adequate charge delivery to the active sulfur particles. Another big question of the sulfur-solid electrolyte interface that needs to be answered regarding the sulfur-solid electrolyte interface is how to overcome the large activation energy for lithium-ion diffusion through sulfur particles that are electrical insulators. In the sulfur electrode's solution-based electrochemical process, the dissolution of the outer part of sulfur particles via Li-PS formation exposes the inner region of the sulfur particles to the liquid electrolyte, which keeps creating a new electrochemical interface. This Li-PS-based reaction is kinetically much faster than the process that provides lithium-ion diffusion through sulfur particles [52], but this fast reaction pathway is not available in the solid-state Li/S cells due to the absence of liquid electrolyte at the sulfur-electrolyte interface. Furthermore, even if a rational sulfur-solid electrolyte interface is initially designed and fabricated, the volume change of sulfur particles during lithiation/delithiation processes [53] can cause severe mechanical deformation of the sulfur-solid electrolyte interface, leading to substantial performance degradation of solid-state Li/S cells.

Hence, a deeper understanding of the interfacial structures from a morphological and chemical perspective is critical for enhancing the performance of Li/S cells and strategically designed advanced solid-state Li/S cells. [54–55] (Figure 1) In this review, we scrutinize the recent progress of solid-state Li/S cells with highlights on advanced

approaches to resolving the issues related to the interfaces between electrodes and electrolytes. Especially recent efforts to overcome the chemical instability issue and inhomogeneous lithium stripping/plating issue at the lithium anode/SSE interfaces and mechanical/chemical approaches to establish percolation paths for Li-ion and electron at the sulfur cathode/SSE interface are examined. In addition, electrochemical analysis and advanced characterization techniques relevant to the investigations of solid-state Li/S cells and their engineered interfaces are discussed. In the concluding remarks, the future directions for the optimization of the electrolyte/electrode interface will be suggested.

## 2 | INTERFACIAL DESIGN OF SOLID-STATE LI/S CELLS

The rational design of solid-state Li/S cells can be implemented by carefully selecting electrodes and solid electrolytes. A material perspective of the respective components is discussed in the above section and is well-reviewed in several papers. [56–61] This section focuses more on the interfacial design and implementation, considering each component of the cells and critical factors that determine the cycling performance. The typical structure of the Li/S cells naturally involves two interfaces in the cell: (1) negative electrode/electrolyte interface and (2) positive electrode/electrolyte interface. The Li metal electrode became a major research interest for many researchers, primarily due to its high theoretical capacity (3860 mAh/g) and large negative potential (-3.06 vs. NHE). [62] Indeed, many Li/S cell studies adopted similar interfacial design strategies of the lithium metal anode as those in the lithium metal cells accompanied by transition metal oxide cathodes. Hence, notable approaches for modifying lithium anodes discussed in this section will not be limited to solid-state Li/S cells. In addition, distinctive methods to fabricate a rationally designed sulfur composite electrode will also be introduced and discussed.

### 2.1 | Morphological design of the electrode/solid electrolyte interface

Forming an adequate electrode/electrolyte interface where electrochemical reactions occur is essential to achieve promising electrochemical performances of solid-state Li/S cells. Unlike Li/S cells with a liquid electrolyte that spontaneously forms the solid-liquid electrochemical interface, developing an effective initial solid-solid interface is very challenging. Also, effective modification methods that can maintain good interfacial contact are often

required due to the electrodes' structural changes caused by the stripping and plating behavior of the lithium metal anode<sup>[63–64]</sup> and the volume changes of sulfur particles in the sulfur electrode occurring during cell operation. Lithium metal solid-state cells, including the Li/S system, generally use a planar lithium metal anode forming an initial planar lithium anode/solid electrolyte interface. Still, microscopic flaws or defects that pre-exist at the interface can promote the formation and propagation of lithium dendrites when the applied current density is above a critical value, which results in an internal short circuit and cell failure, according to Y-M Chiang et al.<sup>[65]</sup> Their work showed that the onset of lithium penetration through the solid electrolyte microstructure strongly depends on its surface morphology, particularly the defect size and density.

Most stabilization strategies of the lithium metal anode focus on chemical modification such as an artificial SEI or surface buffer layer, which mitigates lithium dendritic growth or any problematic chemical reactions between lithium metal and solid electrolytes. Those chemical modification methods will be discussed separately, but there are also notable discoveries about the importance of the lithium/solid electrolyte interfacial microstructure discussed below. Tu et al. reported the effect of initial surface irregularities (e.g., cracks and voids) on lithium deposition using the model geometry in which a small interface irregularity is created at the surface of the solid electrolyte.<sup>[66]</sup> In that work, it was assumed that the initial contact between lithium metal and solid electrolyte is perfect and the total current applied at the bottom boundary is constant. The results indicate that current is concentrated near the defect at the interface and causes an uneven current density distribution. However, the current perturbation affected by defects can be mitigated when the size of the defect (in terms of width and length) is sufficiently reduced, e.g. the defect with 40 nm width and 100 nm length perturbs the current density only within  $|x| < 0.2 \mu\text{m}$ , according to their results. The author suggested that a “shallow and wide” defect will be less impactful to the lithium deposition stability than a “deep and narrow” defect, and an uncontrolled defect at the lithium/solid electrolyte interface can promote problematic dendrite formation of lithium metal. The modeling results suggest that the initial surface morphology of the lithium metal anode plays a vital role in stabilizing lithium deposition behavior. Thus surface engineering methods such as mechanical,<sup>[64,67–74]</sup> or electrochemical polishing<sup>[75–76]</sup> for lithium metal (or solid electrolyte) which smoothes the lithium/solid electrolyte interface or removes undesirable surface residues needs to be considered. Although the polishing effect of lithium metal anode for lithium metal solid-state cells has rarely been investi-

gated, it is worthwhile introducing some reports that evaluate mechanically or electrochemically surface-polished lithium anodes for conventional lithium-ion cells with liquid electrolytes.<sup>[64,76]</sup> Those results show that a surface-smoothed, fresh lithium surface homogenizes lithium deposition behavior, stabilizing the electrochemical behavior of the lithium anode in the lithium-ion cells. The mechanical polishing process using silicon carbide paper with the assistance of acetone results in a macroscopically flat and clean initial surface of the lithium metal. The mechanically polished lithium metal electrode showed very smooth, dendrite-free lithium deposits during lithium stripping/plating processes.<sup>[64]</sup> The electrochemical polishing process that smooths the lithium metal surface via anodic dissolution followed by forming a smooth solid electrolyte interphase (SEI) surface layer was also demonstrated to be a well-developed method for lithium metal surface finishing. The electrochemically polished lithium metal anodes exhibited significantly enhanced cycling stability over 200 cycles at a current density of  $2 \text{ mA/cm}^2$ .<sup>[76]</sup>

In lithium metal solid-state cells, a surface polishing process is generally performed for the surface of the solid electrolytes facing the lithium metal anode because the surface of the pelletized solid electrolyte tends to be very rough. The rough interface may create microscopic voids at the lithium/solid electrolyte interface and degrades the contact between lithium metal and solid electrolyte. In addition, it was found that some solid electrolytes have an undesired chemical surface layer that has different physicochemical properties from the intrinsic properties of the solid electrolyte. For example, the garnet-type electrolytes are generally reactive with humid air, and they form a thin  $\text{Li}_2\text{CO}_3$  layer on their surface when exposed to humid air.<sup>[74,77]</sup> The lithiophilic property of the garnet-type solid electrolyte is then hindered by the lithiophobic  $\text{Li}_2\text{CO}_3$  layer, which increases interfacial resistance at the lithium /garnet-electrolyte interface. According to a previous report, the lithium-LLZO interfacial resistance is significantly increased when the LLZO is exposed to air for 24 h or longer and surface polishing can reduce the interface resistance.<sup>[77]</sup> Several research papers also reported that the wetting property of molten lithium is significantly improved after the surface of the garnet-type solid electrolyte is polished and often followed by thermal treatment.<sup>[67,69–71,73–74]</sup> Sakamoto et al.<sup>[70]</sup> investigated the effect of dry polishing, wet polishing, and those combined with post-heat-treatment on the wetting properties of molten lithium to the LLZO. They demonstrated very low interfacial resistances of only  $2 \Omega \text{ cm}^2$  after wet polishing and heat-treatment at  $500^\circ\text{C}$ , comparable to that of the solid-liquid electrolyte interface in lithium-ion cells. The improved interface almost doubled the critical current density and successfully showed stable galvanostatic

cycling behavior for 100 cycles with no sign of short-circuiting.

While a planar and smooth lithium/solid electrolyte is generally preferred, there have been some attempts to develop a 3D lithium/solid electrolyte structure.<sup>[78–80]</sup> Cui et al. reported a lithium metal solid-state cell that employs a 3D lithium anode consisting of infiltrated lithium metal into 3D reduced graphene oxide (rGO).<sup>[80]</sup> The key idea of this approach is to reduce the effective current density and mitigate the effect of the volumetric changes of lithium metal by accommodating lithium metal in the 3D micro-architecture of the rGO so that electrochemical reaction kinetics and interfacial durability of the lithium anode can be improved. A flowable polymer electrolyte interphase was used to fill the pores of the 3D lithium/rGO anode for intimate contact between the 3D lithium anode and the LLZTO solid electrolyte. Notably, the lithium metal solid-state full cells exhibited a specific capacity of 141 mAh/g and capacity retention of 93.6% after 300 cycles at a 1 C rate at 80°C. Zhang et al. reported an intercalated composite solid electrolyte consisting of layered lithium montmorillonite, poly(ethylene carbonate), lithium bis(fluorosulfonyl)imide, high-voltage fluoroethylene carbonate additive, and poly(tetrafluoroethylene) binder.<sup>[78]</sup> The composite solid electrolyte exhibits an ionic conductivity of  $10^{-4}$  S/cm, a stable electrochemical window of up to 4.6 V, and a lithium-ion transference number of 0.83.

The composite solid electrolyte showed improved electrochemical stability in symmetric lithium cells with a stable voltage plateau for 315 hours during a galvanostatic cycling test at 0.5 mA/cm<sup>2</sup>. The lithium metal cell employed conventional organic liquid electrolyte showed stable electrochemical behavior for only 43 h. Interestingly, the symmetric lithium cell with the 3D lithium anode consisting of the lithium metal infiltrated into the 3D nickel foam current collector showed much better electrochemical stability than the cell with the planar lithium electrode, where very stable voltage curves were observed even after 600 hours. Initial interfacial resistance of the 3D lithium anode was 106  $\Omega$  that is slightly lower than that of the planar lithium anode (118  $\Omega$ ), but the interfacial resistance of the planar lithium anode increased dramatically to 404  $\Omega$  after 100 cycles whereas that of the 3D lithium anode increased to 255  $\Omega$ . It was also shown that the top surface of the 3D lithium anode was dendrite-free and much smoother than those of the planar lithium anode tested in the lithium metal/LiFePO<sub>4</sub> full cells for 200 cycles, indicating the effect of the 3D anode in stabilizing lithium metal stripping/plating behavior.

A 3D mixed electron/ion conducting framework (3D-MCF) consisting of a tape cast, tri-layered (porous-dense-porous) garnet electrolyte with a carbon nanotubes (CNTs)

coating on the surface of the garnet electrolyte and lithium metal infiltrated into the garnet-CNT scaffold was reported by Hu et al.<sup>[81]</sup> (**Figure 2**). The conformal coating of CNTs on the porous internal structure of the garnet solid electrolyte not only creates an effective electronic/ionic conduction pathway but also serves as a host for lithium metal infiltration. Improved lithium symmetric cell cycling behavior at a current density of 3 mA/cm<sup>2</sup> with a controlled capacity of 3 mAh/cm<sup>2</sup> was achieved with the 3D-MCF cell, and no significant development of overpotential was observed after 140 hours of lithium stripping and plating processes, indicating the high current density operation capability of the 3D-MCF cells.

The microstructure of the sulfur electrode/solid electrolyte interface is more complicated than that of the lithium anode/solid electrolyte interface because the sulfur electrode generally forms a porous microstructure consisting of the interconnection of multiple solid components such as active sulfur particles, functional additives, and a polymeric binder. In conventional lithium/sulfur cells employing an organic liquid electrolyte, the continuous pore channels of the sulfur electrode filled with liquid electrolyte serve as a lithium-ion conduction pathway from the bulk electrolyte to the internal structure of the sulfur electrode. In solid-state Li/S cells, the conduction pathway of lithium-ions is established via interconnection of the solid electrolyte particles, and adequate physical contact between solid sulfur and solid electrolyte must be formed, implying that the design strategies of the sulfur electrode/solid electrolyte interface are crucial to achieving practically attractive electrochemical performance. The cold-pressing technique has been commonly used to improve interfacial contact between the sulfur electrode and solid electrolyte.<sup>[82–85]</sup> There are a few different approaches to perform the cold pressing technique to engineer the sulfur cathode/solid electrolyte interface. One common way is to add the sulfur-carbon composite powder to the pelletized solid electrolyte and press them together to compact the electrode/electrolyte interface. The cold pressing process of the pelletized solid electrolyte and the sulfur composite electrode effectively reduces the interfacial resistance between the sulfur electrode and solid electrolyte, but it does not form an electrochemical interface adequately unless the solid electrolyte powder is homogeneously distributed within the sulfur electrode.

More recently, researchers have started directly incorporating solid electrolyte powder into the sulfur composite cathode to construct an effective ionic conduction pathway in the sulfur electrode.<sup>[86–92]</sup> During the sulfur electrode fabrication process, solid electrolyte powder is added to the slurry and homogeneously mixed with them before casting onto a metallic current collector or one side of the solid electrolyte pellet to form a sulfur electrode.

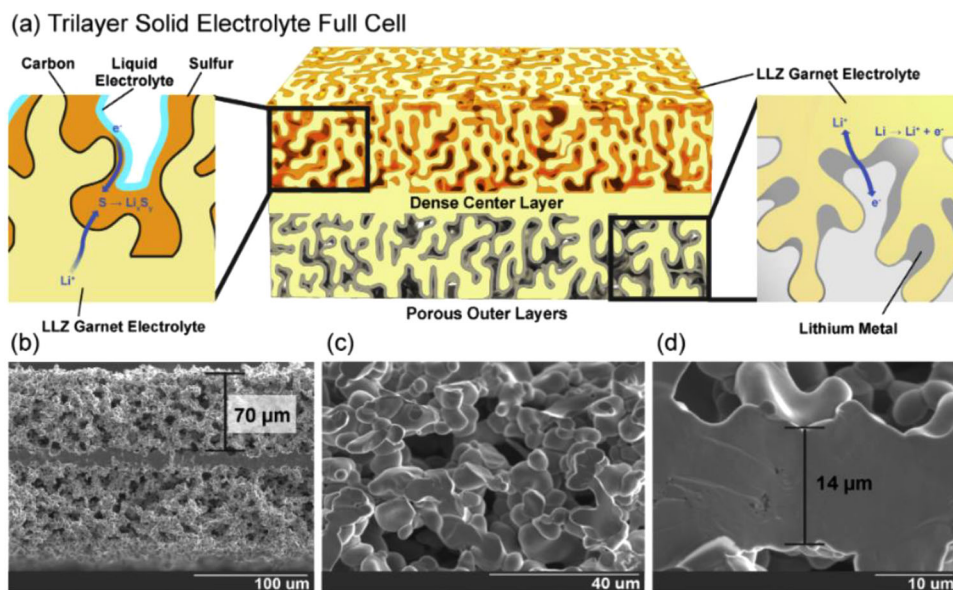


**FIGURE 2** (a) Diagram of a trilayer lithium/garnet/sulfur cell with high interfacial surface area, short lithium-ion conduction pathways, and minimized use of liquid electrolyte. (b) SEM cross-section of the porous-dense-porous trilayer after binder burnout and sintering. Magnified SEM (c) of the porous layer with high porosity and high interconnectivity and (d) the thin, dense blocking layer of a sintered trilayer cell.<sup>[81]</sup>

Mechanical ball milling is also often used to mix the sulfur and solid electrolyte particles.<sup>[86–91]</sup> The effect of the mechanical ball milling was investigated by Tatsumisago et al.<sup>[89]</sup> by comparing the electrochemical behavior of the Li/Li<sub>2</sub>S cells to solid-state cells prepared via different mixing processes of the sulfur, carbon, and 80Li<sub>2</sub>S–20P<sub>2</sub>S glassy ceramic solid electrolyte (SE). Three composite electrodes were prepared: (1) “Li<sub>2</sub>S + acetylene black (AB) + SE” was prepared by hand grinding Li<sub>2</sub>S, carbon, and solid electrolyte; (2) “Li<sub>2</sub>S–AB + SE” was obtained by ball milling a mixture of Li<sub>2</sub>S and carbon, and then hand-grinding the ball-milled Li<sub>2</sub>S–AB and the solid electrolyte; (3) “Li<sub>2</sub>S–AB–SE” electrode was obtained by milling a mixture of the Li<sub>2</sub>S–AB composite and the solid electrolyte. The Li<sub>2</sub>S–AB–SE electrode demonstrated the best electrochemical performance with a specific capacity of 700 mAh/gS at 0.064 mA/cm<sup>2</sup>. In contrast, the other two electrodes showed low specific capacities of less than 200 mAh/gS at the same applied current density. Cross-sectional TEM observations of the Li<sub>2</sub>S–AB–SE composite revealed its nanostructure comprised of the nano-sized Li<sub>2</sub>S particles and carbon particles surrounded by the solid electrolyte. The authors suggested that the ball milling process not only forms adequate contact between the active Li<sub>2</sub>S and solid electrolyte but also reduces the particle size of Li<sub>2</sub>S, which promotes the electrochemical reaction rate and improves the specific capacity of the solid-state Li/Li<sub>2</sub>S cells. Fan et al.<sup>[91]</sup> employed both ball milling and cold pressing techniques to further improve sulfur/solid electrolyte interfacial structure. In their work,

the synthesized Li<sub>10</sub>SnP<sub>2</sub>S<sub>12</sub> solid electrolyte powder and the ball-milled sulfur-carbon composite (2:1 w/w) were ball milled at 370 rpm for 1 h with a different weight ratio of S:Li<sub>10</sub>SnP<sub>2</sub>S<sub>12</sub>:C = y:(100–1.5y):0.5y, where y (sulfur content) = 20, 25, 30, and 35. The prepared cathode-solid electrolyte composite was spread on one side of the solid electrolyte pellet and cold-pressed to form good interfacial contact. All cells prepared with different sulfur content exhibited a high initial discharge capacity of about 1500 mAh/gS at 40 mA/g. The cell with higher sulfur content tended to decay faster, which might be due to the more severe volume and stress/strain changes of the sulfur cathodes with higher sulfur contents. The author reported the sulfur content of 25 wt % to be an optimal content, and the optimized solid-state Li/S cell (25 wt.% S) exhibited a good cycling performance for 50 cycles and a rate capability of up to 320 mA/g.

For Li/S cells with organic liquid electrolytes, it is known that the existence of lithium polysulfide (Li-PS) in the liquid organic electrolyte can lower the high activation energy required to delithiate Li<sub>2</sub>S during the charging process of the Li<sub>2</sub>S electrode.<sup>[93–94]</sup> However, the fact that Li-PS does not exist in the solid-state raises an essential question about how the high activation energy of Li<sub>2</sub>S for delithiation can be overcome without Li-PS at the Li<sub>2</sub>S/solid-electrolyte interface. Wagemaker et al. investigated the interface of Li<sub>6</sub>PS<sub>5</sub>Cl/Li<sub>2</sub>S using the NMR exchange technique<sup>[52]</sup> and found that the major hurdle of the electrochemical process of Li/S solid-state cells is the interfacial resistance between Li<sub>2</sub>S and the solid

electrolyte, which limits the power performance of the present Li/S solid-state cells. It was suggested that interfacial design of sulfur/solid electrolyte and reducing the particle size of sulfur active material should be considered one of the main directions to improve solid-state cell performance. In addition, the development of interfacial resistance during cell operation caused by interfacial changes should be regarded as one of the main reasons for cell performance degradation of the Li/S solid-state cells. Liang et al. reported that the nanoconfinement of  $\text{Li}_2\text{S}$  particles improves ionic conductivity of  $\text{Li}_2\text{S}$  by two orders of magnitude compared to the bulk  $\text{Li}_2\text{S}$  particles.<sup>[52,95]</sup> Nano-sized  $\text{Li}_2\text{S}$  particles were synthesized via the wet chemical method, and a superionic conductor,  $\text{Li}_3\text{PS}_4$  was coated onto the surface of  $\text{Li}_2\text{S}$  nanoparticles by exposing the surface of the nano  $\text{Li}_2\text{S}$  with  $\text{P}_2\text{S}_5$ , which further improves the ionic conductivity of nano  $\text{Li}_2\text{S}$  by four orders of magnitude (from  $10^{-11}$  to  $10^{-7}$  S/cm at  $25^\circ\text{C}$ ). Improved specific capacity and cyclability of the  $\text{Li}_3\text{PS}_4$  coated nano  $\text{Li}_2\text{S}$  cathode (848 mAh/g  $\text{Li}_2\text{S}$ ) for the solid-state Li/ $\text{Li}_2\text{S}$  cells were demonstrated at 0.1 C at  $60^\circ\text{C}$  compared to the bare nano  $\text{Li}_2\text{S}$  cathode (569 mAh/g  $\text{Li}_2\text{S}$ ). After 100 cycles, a specific capacity of the  $\text{Li}_3\text{PS}_4$  coated nano  $\text{Li}_2\text{S}$  cathode higher than 600 mAh/g  $\text{Li}_2\text{S}$  was still obtained, while the bare nano  $\text{Li}_2\text{S}$  retained approximately 400 mAh/g  $\text{Li}_2\text{S}$ . It was also noted that the bulk  $\text{Li}_2\text{S}$  cathode did not show meaningful electrochemical behavior due to its large particle size and poor ionic conductivity.

Recently, there have been some attempts to build a 3D sulfur/solid electrolyte interface that reduces interfacial resistance, builds fast and continuous long-range electron-ion transport pathways, and improves the stability of the electrode/electrolyte interface.<sup>[23,81,96–98]</sup> Zhang et al. developed a Li/S solid-state cell consisting of a  $\text{Li}_{0.33}\text{La}_{0.557}\text{TiO}_3$  (LLTO) nanofiber-polyethylene oxide (PEO) solid composite electrolyte and a sulfur/carbon nanofiber (CNF/S) cathode whose pores are filled with PEO.<sup>[93]</sup> The LLTO nanofiber in the composite solid electrolyte system stabilizes the lithium stripping/plating behavior of the lithium metal anode compared to the PEO solid electrolyte in the lithium symmetric cell test, where much lower voltage ( $>0.2$  V) and longer stability of over 1000 hours (vs. 200 hours of the PEO electrolyte) without the development of overpotential. The author suggested that the improved electrochemical behavior of the symmetric lithium cells of the composite electrolyte system was attributed to the continuous ionic transport pathway through 1D structured LLTO and the good mechanical stability of the polymer/ceramic composite system. The solid-state Li/S cell fabricated with the PEO-LLTO/S-CNF bilayer demonstrated good cycling performance for 40 cycles at 0.05 C at room temperature with Coulombic efficiency over 99% after 50 cycles, although its sulfur uti-

lization is not high enough (approximately 400 mAh/g S was reported). A 3D stainless steel current collector for the  $\text{Li}_2\text{S}$ -solid electrolyte ( $\text{Li}_3\text{PS}_4$ ) composite cathode for the solid-state Li/S cells reported by Wang and co-workers<sup>[97]</sup> also showed promising initial specific energy of 370 Wh/kg for the first cycle. According to the results, the 3D porous stainless steel current collector efficiently accommodates a  $\text{Li}_2\text{S}$  mass loading from 2.54–7.64 mg/cm<sup>2</sup> without losing obtainable specific capacity, which is attributed to the effective electronic conduction pathway of the sulfur electrode provided by the electronically conductive 3D scaffold of the stainless steel current collector. Rate capability tests of up to 0.5 C and cyclability for 100 cycles with a specific capacity of about 500 mAh/g  $\text{Li}_2\text{S}$  were demonstrated at  $25^\circ\text{C}$  using the  $\text{Li}_2\text{S}$  electrode ( $\text{Li}_2\text{S}$  mass loading of 2.54 mg/cm<sup>2</sup>).

A unique approach to constructing a dense/porous bilayer structure of the garnet-type solid electrolyte was suggested by Hu and co-workers.<sup>[23,81,98]</sup> In one of their works,<sup>[23]</sup> the dense  $\text{Li}_7\text{La}_{2.75}\text{Ca}_{0.25}\text{Zr}_{1.75}\text{Nb}_{0.25}\text{O}_{12}$  (LLCZNO) layer was fabricated using the tape casting method with an assist of polymer binder, while the same method was used to prepare the porous layer except for that spherical poly(methyl methacrylate) (PMMA) powder was added to the slurry. The prepared dense LLCZNO layer and the PMMA-containing LLCZNO layer were laminated and hot-pressed at  $80^\circ\text{C}$  for 2 h to form a good connection at their interface. Finally, the sintering process was performed at  $700^\circ\text{C}$  for 4 h to remove all volatile components in the hot-pressed bilayer, which leaves a porous structure in the PMMA-containing LLCZNO layer. This composite is then further sintered at  $1100^\circ\text{C}$ . The thick, porous layer has continuous  $\text{Li}^+$  / electron pathways to host the sulfur cathode. The thin dense layer additionally impedes Li dendrite formation. The sulfur electrode is formed in the porous LLCZNO layer by casting CNT ink followed by thermal sulfur infiltration. Although the cell tested in this work used some amount of liquid electrolyte to promote the kinetics of the electrochemical process, the cell showed a capacity of higher than 600 mAh/gS with a sulfur mass loading of 7.5 mg/cm<sup>2</sup> and an average Coulombic efficiency of 99% during a galvanostatic cycling test. The specific capacity of the Li/S hybrid cells was further improved to about 1200 mAh/gS in their following work.<sup>[81,98]</sup>

## 2.2 | Chemical interfacial design

Solid-state Li/S cells are free from the primary concern of the liquid electrolyte Li/S cells, particularly the shuttling of the Li-PS. However, most solid electrolytes still suffer from low conductivity compared to their organic liquid electrolyte counterparts primarily due to high interfacial

impedance developed by poor interfacial contact, significant microstructural instability, dendrite formation during Li plating/stripping, and chemical stability problems. Especially, the lithium dendrite growth issue at the negative electrode still persists with inorganic solid electrolytes and predominantly occurs at cracks, defects, and grain boundaries of the solid electrolytes or where free electrons are trapped.<sup>[99]</sup>

Chemical modification or coating of a buffer layer on the electrode or electrode/electrolyte interfaces can be viable methods to address these issues. Several investigations have been performed on the stabilization of lithium metal anodes, such as forming an artificial SEI layer or surface buffer layer to reduce the interfacial impedance and mitigate the unnecessary side reactions to enhance the cycling efficiency of the cell. In both cases, it is crucial to employ a surface coating material that is highly conductive for lithium-ions while chemically/electrochemically stable with the electrode materials, that is, lithium and sulfur.

Non-lithiated or lithium-free metal and metal oxide layers can serve as such layers. In most cases, the non-lithium metal is deposited on the surface of a lithium metal anode and forms a partially lithiated interface that promotes lithium-ion transport as well as achieving good interfacial contact. Fu et al.<sup>[24]</sup> engineered the surface of a garnet-type solid electrolyte (LLCZN) to form an intermediary Li-metal alloy to generate a lithiophilic interface. The results showed a major decrease (from 950  $\Omega$  cm<sup>2</sup> to 75  $\Omega$  cm<sup>2</sup>) due to the changes in the wettability of the garnet surface.<sup>[24]</sup> Similarly, Han et al.<sup>[101]</sup> reported an ultrathin Al<sub>2</sub>O<sub>3</sub> coating on lithium metal anode using atomic layer deposition (ALD), and then the anode was placed in contact with garnet-like Li<sub>7</sub>La<sub>2.75</sub>Ca<sub>0.25</sub>Zr<sub>1.75</sub>Nb<sub>0.25</sub>O<sub>12</sub> (LLCZN) solid electrolytes.<sup>[101]</sup> The metal oxide coating on the anode surface aids wetting of the metallic lithium, and the lithiated-alumina interface formed during the ALD deposition step allows effective lithium-ion transport between the anode and the garnet electrolyte. As a result, a significant decrease of the area-specific interfacial impedance was observed, from 1710  $\Omega$  cm<sup>2</sup> to 1  $\Omega$  cm<sup>2</sup> at room temperature after Al<sub>2</sub>O<sub>3</sub> deposition. A sputter-coated thin gold layer film also served as a lithiophilic buffer layer.<sup>[102–103]</sup> The uniformly sputtered Au layers formed an alloy with Li at room temperature once the electrolyte was bonded to the lithium foil. This alloy layer enhances conformal contact between the lithium anode and the electrolyte. Also, the Au layer helps redistribute the Li<sup>+</sup> to promote uniform Li metal deposition. Consequently, the interfacial impedance measured in a Li symmetric cell showed a remarkable decrease from ~3000  $\Omega$  cm<sup>2</sup> to 380  $\Omega$  cm<sup>2</sup> after Au coating.

Polymer electrolytes are other candidates that can impart excellent wettability to the lithium metal anode

surface and uniform Li deposition. Since polymer processing does not require high vacuum deposition steps, polymer coatings are advantageous in accessibility and scalability. Several studies reported a surface coating of the lithium metal anode with lithium conducting polymer electrolytes to enhance the interfacial contact and reduce the interfacial impedance. Wang and co-workers used poly(ethylene oxide) (PEO) mixed with lithium bis(trifluoromethanesulfonyl)imide (LiTFSI) as a buffer layer between electrodes and solid electrolytes. The solid polymer electrolyte (SPE) coating layer enables an improved interfacial property between the electrolyte and electrodes. A symmetric lithium cell exhibited stable cycling performance, and the solid-state lithium-sulfurized polyacrylonitrile (SPAN) battery delivers an ultrahigh initial discharge capacity of 1793 mAh/g at 75°C, which is beyond the theoretical specific capacity of sulfur electrode.<sup>[21]</sup> Authors suggested the specific capacity higher than the theoretical maximum of a sulfur electrode is due to the contribution of  $\pi$ -conjugated pyridinic carbon framework to the Faradaic processes and a non-Faradaic pseudocapacitance that may persist over many cycles.<sup>[104]</sup> Liu and co-workers grafted a Tween-20 polymer onto the lithium metal anode surface, which served as a polymeric interfacial layer and suppressed the contact and reaction between polysulfides and the lithium metal.<sup>[105]</sup> The tween polymer interfacial layer improved the compatibility of the Li/electrolyte interface, which enables low overpotential and stable performance over 1000 cycles. The resulting quasi-solid-state full cell exhibited capacities of 1051.2 mAh/g at 0.2 C, and good stability for 500 cycles at 2 C. X-ray photoelectron spectroscopy (XPS) revealed that the polymer interfacial layer also suppresses polysulfide reduction on the metallic Li surface even after long-term cycling.<sup>[105]</sup>

Lithium-rich compounds such as lithium salts, especially LiF or Li<sub>3</sub>PO<sub>4</sub>, also served as good surface coating layers owing to their good chemical stability. Fan et al. coated the lithium metal anode with a LiF-rich solid electrolyte interphase (SEI) layer formed by an in-situ method.<sup>[106]</sup> The LiF-rich artificial SEI successfully suppressed Li dendrite growth, and the low electronic conductivity of LiF blocked the (undesired) side reactions between the SSEs and Li metal. The critical current density of LPS SSE increased from 0.7 mA/cm<sup>2</sup> to 2 mA/cm<sup>2</sup> at room temperature after the coating was applied.<sup>[106]</sup> Chen and coworkers reported an effective strategy to stabilize the Li metal anode by in situ constructing an antimony-based lithiophilic interphase on the Li anode (Sb-Li) using an antimony triiodide-tetrahydrofuran (THF) solution. The Sb-Li anode enables dendrite-free Li deposition in both ether- and ester-based electrolytes. The assembled Li-S cells exhibited an initial capacity of 915 mAh/g at 1.0 C

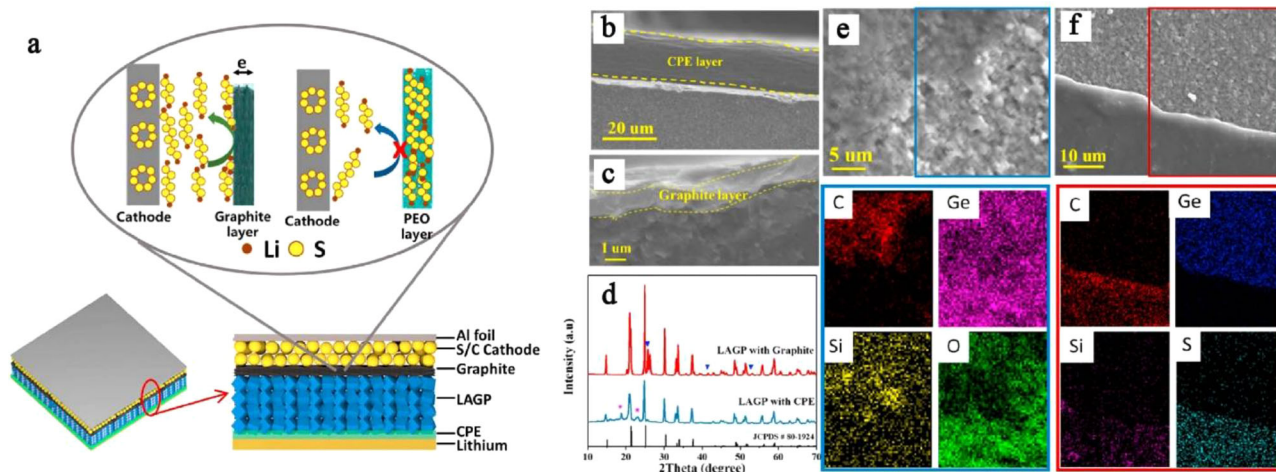


**FIGURE 3** (a) The surface modification strategies applied to lithium anode and sulfur cathode interfaces. A composite polymer electrolyte buffer layer (b) and a graphite conductive layer (c) are successfully formed on the LAGP solid electrolyte. (d) X-ray diffraction data of the solid electrolyte with protective layers. (e, f) SEM/EDX elemental mapping images of LAGP ceramic SE covered with (e) graphite and (f) polymer electrolytes.<sup>[100]</sup>

and capacity retention >83% after 400 cycles.<sup>[107]</sup> Deng et al. reported infusing garnet-type solid electrolytes with air-stable electrolyte,  $\text{Li}_3\text{PO}_4$  (LPO), which significantly reduced interfacial resistance to  $1 \Omega \text{ cm}^2$  and achieved a high critical current density of  $2.2 \text{ mA/cm}^2$ . The coated LPO electrolyte showed robust mechanical strength and ion conductivity. The electronically insulating property of LPO provided suppression of Li dendrite growth and the direct reduction of the electrolyte.<sup>[108]</sup>

Investigations of chemical modification of the cathode-solid electrolyte interface are more scarce than those concerned with the anode interface due to the nature of the granular-type sulfur electrode architecture. The interfacial design efforts focus on microstructural design, which was reviewed in the above section. However, a few examples report the chemical modification of the cathode surfaces provided below. Manthiram and coworkers employed a thin polymer with intrinsic nanoporosity (PIN), which is a class of polymeric materials that possess a rigid backbone structure, coated on a NASICON-type  $\text{Li}_{1+x}\text{Al}_x\text{Ti}_{2-x}(\text{PO}_4)_3$  (LATP) solid electrolyte. The PIN layer that served as a molecular sieve layer can efficaciously prevent the migration of polysulfide species while permitting the transport of lithium ions. At the sulfur electrode side, the PIN layer not only prevents the migration of polysulfides to the surface of LATP but also prevents the reduction of LATP while maintaining an adequate ionic interface between the sulfur-carbon composite cathode and the LATP membrane. The  $\text{Li}||\text{PIN-LATP}||\text{S/C}$  cell exhibited a specific capacity of  $950 \text{ mAh/gS}$  at  $0.2 \text{ C}$ , comparable to the case of a cell separated by a commercial membrane.<sup>[109]</sup> Li et al. reported coating of the sulfur electrode with an electronically conductive graphite layer. (**Figure 3**) This layer demonstrated

improvement in the utilization of active sulfur by providing redox reaction sites. Furthermore, the graphite can confine the reduced production of  $\text{S}_8$  within the conductive network and serve as a second current collector. The interface-modified Li/S cell exhibited good cycle stability ( $1080 \text{ mAh/gS}$  after 150 cycles) and high Coulombic efficiency of 96%.<sup>[100]</sup> Sun et al. employed ionic liquid (IL) as interfacial modification of the cathode.<sup>[110]</sup> They observed a significant decrease of interfacial resistance from  $3540$  to  $39 \text{ Ohm/cm}^2$  in the symmetric cell. Solid-state Li/S cells fabricated with a garnet electrolyte coated with IL showed a specific capacity of  $340 \text{ mAh/gS}$  that provides electrochemical and physical stability during cycling.<sup>[110]</sup>

### 3 | CHARACTERIZATION METHODS FOR ELECTRODE/SOLID ELECTROLYTE INTERFACES

Despite the significant progress in developing solid superionic conductors for solid-state lithium/sulfur cells in recent decades, there are still unresolved issues associated with their chemical or structural instabilities in solid-state Li/S cells. Their excellent ionic conductivity cannot be utilized for the fast electrochemical process of solid-state Li/S cells unless their structural and interfacial integrities are preserved during cell operation. Electrochemical methods are potent tools for probing chemical reactions involving charge transfer at electrode/electrolyte interfaces. Electrochemical techniques can detect interfacial changes that influence the performance of solid-state Li/S cells, so electrochemical analysis is an essential tool in developing long-term durable solid-state Li/S cells. However, due to the

complexity of the solid-state Li/S cell, consisting of multiple solid constituents with complex interfacial microstructures participating in the electrochemical process, current or voltage responses obtained by electrochemical techniques cannot be interpreted unless proper physical or chemical characterizations are also used. Optical and electron microscopies, chemical spectroscopies such as NMR, and X-ray-based techniques are generally performed to investigate electrochemical interfaces before and after electrochemical processes to complement electrochemical characterization. In addition, researchers have also developed unique in situ/in operando techniques for more detailed investigation and intended to make the electrochemical environment of the testing chambers representative of actual battery cells.<sup>[111]</sup>

Like other lithium rechargeable batteries, the galvanostatic charge/discharge cycling test at a given current density over a controlled voltage window is perhaps the most important electrochemical qualification method for Li/S solid-state cells. During the galvanostatic cycling test, solid-state Li/S cells are repeatedly charged and discharged at a constant applied current to demonstrate their electrochemical performance in cell capacity, nominal voltage, and Coulombic efficiency and monitor their changes during cycling. The capacity of the cells is generally determined when the discharge voltage declines and the internal cell resistance increases steeply, respectively, and reaches the cut-off voltage set for the cycling test. Potentiodynamic polarization techniques where the electrode's potential is varied linearly at a selected scan rate (V/s) are also helpful electrochemical methods for Li/S solid-state cells.

Potentiodynamic polarization techniques can evaluate the potentials for the redox reactions and their reaction kinetics and reversibility at a given voltage scan rate (V/s).<sup>[112]</sup> The most straightforward potentiodynamic technique is linear sweep voltammetry (LSV) which scans a given potential range (in one direction) as a linear function of time. Cyclic voltammetry (CV) is a fundamentally similar technique to LSV, but the direction of the potential scan is reversed at the end of each scan. Most of the studies on solid-state Li/S cells performed both galvanostatic cycling test and CV to investigate the effect and failure mechanisms of the interfacial modification or to evaluate their lifespan and reliability of solid-state Li/S cells. Tatsumisago et al.<sup>[89]</sup> showed charge-discharge curves of all-solid-state cells with various Li<sub>2</sub>S-solid electrolyte composite electrodes. The highest specific capacity of about 700 mAh/gLi<sub>2</sub>S is attributed to the most extended discharge voltage plateau, and the minimum overpotential was demonstrated with ball-milled Li<sub>2</sub>S-carbon-Li<sub>2</sub>S-P<sub>2</sub>S<sub>5</sub> composite electrode. In contrast,

the other composite electrodes obtained by hand grinding of Li<sub>2</sub>S (or Li<sub>2</sub>S-carbon) and Li<sub>2</sub>S-P<sub>2</sub>S<sub>5</sub> exhibited very low or almost negligible initial capacities with large overpotential. The authors concluded that the performance enhancement of the ball-milled Li<sub>2</sub>S-carbon-Li<sub>2</sub>S-P<sub>2</sub>S<sub>5</sub> composite electrode was attributed to the improved sulfur/solid electrolyte interface formed via the ball-milling process.

Potentiodynamic polarization techniques are commonly used to determine the electrochemical stability window of solid electrolytes<sup>[78,87,91–92,96,113]</sup> using a cell consisting of a lithium metal electrode, solid electrolyte, and a stainless-steel blocking electrode. The peaks of current in the voltammograms indicate the redox reactions at the electrode/electrolyte interface and are generally associated with the decomposition of the solid electrolyte. By demonstrating the decomposition potential of the solid electrolyte, the electrochemical window for stable electrochemical operation of solid-state Li/S cells can be determined. Zhang et al.<sup>[25]</sup> conducted the LSV method in the potential range from 2 to 5.5 V to determine the electrochemical windows of composite solid electrolytes consisting of poly(ethylene carbonate) (PEC) and lithium bis(fluorosulfonyl)imide (LiFSI) at 25°C.<sup>[78]</sup> They showed that the addition of lithium montmorillonite (LiMNT) to the PEC-LiFSI composite electrolyte stabilizes the composite electrolyte at high (positive) potential, and it was further improved by the addition of poly(tetrafluoroethylene) (PTFE) binder. Tu et al. performed a similar experiment for the sulfide solid electrolyte using the CV technique.<sup>[87]</sup> Their work demonstrated the improved electrochemical window of Li<sub>7</sub>P<sub>3</sub>S<sub>11</sub> solid electrolyte up to 5 V after molybdenum doping of the Li<sub>7</sub>P<sub>3</sub>S<sub>11</sub> solid electrolyte (Li<sub>7</sub>P<sub>2.9</sub>S<sub>10.85</sub>Mo<sub>0.01</sub>), and the slightly unstable current observed during the CV for the Li<sub>7</sub>P<sub>3</sub>S<sub>11</sub> was significantly reduced, indicating improved electrochemical stability of the Li<sub>7</sub>P<sub>2.9</sub>S<sub>10.85</sub>Mo<sub>0.01</sub> (Figure 4).

Studies on the mechanisms of high ionic conduction in solid electrolytes have been very important for solid electrolyte development.<sup>[87,92,95,113–114]</sup> DC polarization methods such as the transient ionic current (TIC) technique<sup>[115–116]</sup> and Wagner's method<sup>[117]</sup> have been widely used to demonstrate ionic and electronic contributions to the total conductivity of solid electrolytes.<sup>[118]</sup> The applied voltage for these techniques must be within an electrochemical window to prevent decomposition of the solid electrolytes. Using data obtained from dc polarization methods, and ionic conduction parameters such as transport/transference number and ionic drift velocity can be measured quantitatively. The Bruce-Vincent method is a modified method to more accurately evaluate the ionic conduction behavior of superionic conductors by combining the dc polarization method

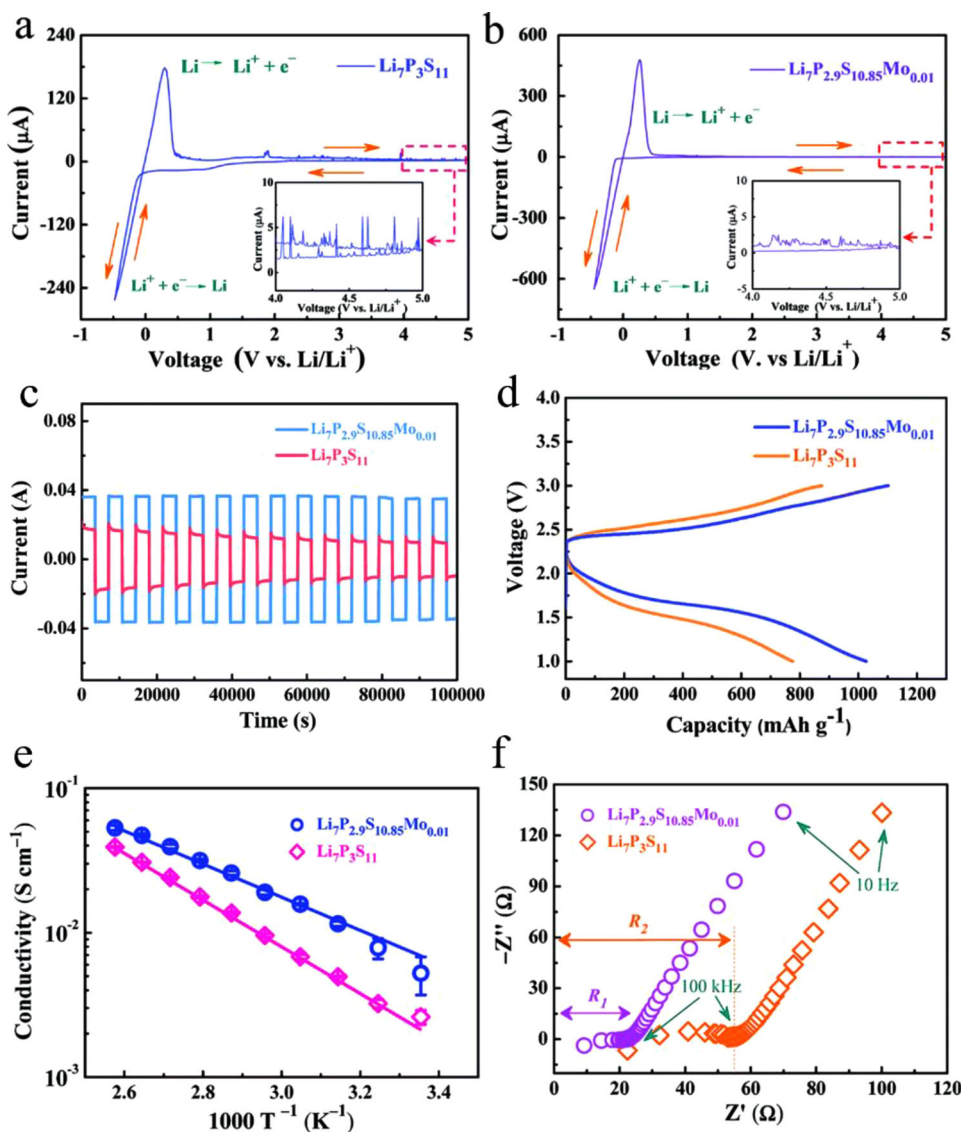


**FIGURE 4** CV curves of (a)  $\text{Li}_7\text{P}_3\text{S}_{11}$  and (b)  $\text{Li}_7\text{P}_{2.9}\text{S}_{10.85}\text{Mo}_{0.01}$  in the potential range from  $-0.5$  V to  $5$  V (vs.  $\text{Li}/\text{Li}^+$ ) at a scanning rate of  $1$  mV/s. (c) DC current curve of  $\text{Li}_7\text{P}_3\text{S}_{11}$  and  $\text{Li}_7\text{P}_{2.9}\text{S}_{10.85}\text{Mo}_{0.01}$  at a constant voltage of  $1$  V. (d) The first cycle charge/discharge voltage profiles of  $\text{Li}_7\text{P}_3\text{S}_{11}$  and  $\text{Li}_7\text{P}_{2.9}\text{S}_{10.85}\text{Mo}_{0.01}$  Li/S cells at a rate of  $C/20$ . (e) Arrhenius conductivity plots. (f) Impedance plots of the electrolytes at room temperature.<sup>[87]</sup>

with the electrochemical impedance spectroscopy (EIS) technique.<sup>[119–120]</sup> The Bruce-Vincent method considers that a real rechargeable cell system is more complicated than the ideal electrochemical system (e.g., more ionic species, residual water, and impurities in the electrolyte). In the case of binary electrolytes (e.g., polymer electrolytes) where both cationic and anionic charge carriers are mobile in the electrolyte phase, the Bruce-Vincent method is conveniently used to determine the cationic current fraction. EIS is generally carried out before and after the dc polarization when the current reaches a steady-state, to consider the parameters associated with a passivation layer formed on the surface of the electrodes.

In the paper authored by Xia et al.<sup>[110]</sup>, the lithium-ion transference number of the PVDF-HFP gel polymer electrolyte (GEP) with a 3D network was evaluated using the Bruce-Vincent method. They demonstrated a lithium-ion transference number of  $0.39$  for the GEP electrolyte comparable with that of liquid electrolyte ( $0.31$ ). The ionic conductivity of solid electrolytes is usually estimated using the Nyquist plot obtained from the EIS of symmetric blocking cells.<sup>[95,113–114]</sup> Cai et al.<sup>[114]</sup> investigated the effect of a 3D framework of  $\text{Li}_{6.4}\text{La}_3\text{Zr}_2\text{Al}_{0.2}\text{O}_{12}$  (LLZAO) in the ionic conductivity of the solid electrolyte. It was demonstrated that the 3D framework of LLZAO improves the ionic conductivity of the composite solid electrolyte

(LLZAO-PEO-LiTFSI) in the temperature range between 30~60°C. High ionic conductivity of the 3D LLZAO-PEO-LiTFSI composite electrolyte up to  $8.62 \times 10^{-4}$  S/cm was demonstrated, which is higher than that of the composite electrolyte without the 3D framework.

EIS is also a potent tool for studying the electrochemical interface of solid-state Li/S cells. Many research articles reported their EIS data to explain the interfacial phenomenon occurring in the solid-state Li/S cells.<sup>[83,84,92,96,121-122]</sup> Because EIS is a non-destructive analysis technique, the electrochemical processes occurring at the interface can be analyzed without destroying the cells. EIS can probe the stability of electrode/solid electrolyte interfaces under various cell operating conditions (e.g., temperature, pressure, and state-of-charge) by monitoring a Nyquist plot or a Bode plot. The internal resistance associated with various electrochemical components such as a surface film (e.g., solid electrolyte interphase) on active materials, charge and mass transfer resistances can be separated from the total internal resistance based on the difference in time constants. Zhang et al.<sup>[92]</sup> shows the changes in the cell impedance of S/Li<sub>6</sub>PS<sub>5</sub>Cl/Li cells before and after the cycle test and proposed an equivalent circuit model accordingly. They showed the large interfacial resistance being developed over 100 cycles (675 Ω) while a relatively small increase in bulk resistance was observed (40 Ω). The authors suggested that this interfacial degradation is the main reason for the subsequent capacity decay of the S/Li<sub>6</sub>PS<sub>5</sub>Cl/Li cells. Narayanan et al. performed an EIS study as a function of the state-of-charge for a mixed conductor composite solid-state electrode/bilayer solid-state electrolyte (CEBE) Li-S cell configuration.<sup>[122]</sup> The bilayer solid-state electrolyte is composed of a PEO-LiTFSI polymer electrolyte and a lithium-ion-intercalating lithium cobalt oxide (LCO) layer, and they intended to use LCO as a facile lithium-ion transport pathway. Interestingly, a lower overall resistance was demonstrated for the CEBE Li/S cells than the Li/S cell with liquid electrolytes. Yang et al. studied the effect of ionic liquid on the interfacial stability of the solid-state Li/Li<sub>10</sub>GeP<sub>2</sub>S<sub>12</sub>(LGPS)/S cells.<sup>[84]</sup> They showed that the addition of 1 M LiTFSI dissolved in N-methyl-N-propylpyrrolidinium bis(trifluoromethanesulfonyl)imide (PYR<sub>13</sub>TFSI) significantly reduces interfacial resistance of the solid-state Li/S cells from 2021 Ω/cm<sup>2</sup> to 142 Ω/cm<sup>2</sup>. The impedance changes of the ionic liquid-containing Li/Li<sub>10</sub>GeP<sub>2</sub>S<sub>12</sub>/S cells were monitored over time for 14 days at open circuit and found that the charge transfer resistance at the lithium metal/LGPS-ionic liquid composite electrolyte interface slightly increased in the first 3 days, implying a formation of an SEI on the lithium metal electrode by the LiTFSI-containing ionic liquid. For the rest of the 12 days, the bulk resistance and charge transfer resis-

tance were almost constant, which indicates a stabilized lithium/LGPS interface.

Because solid-state Li/S cells cannot be free from the problematic issue associated with the lithium/solid electrolyte interface, understanding the failure mechanism of the lithium electrode is essential for developing reliable solid-state Li/S cells. The stability of the solid electrolyte in contact with the lithium metal electrode is normally investigated by electrochemical techniques using a Li/solid electrolyte/Li symmetric cell configuration.<sup>[23,69,79,86,96]</sup> Especially, the symmetric cell cycling test for repeated lithium stripping/plating is very useful to demonstrate how the lithium/solid electrolyte interface changes under electrochemical cycling conditions. Unstable voltage measured during galvanostatic plating-stripping cycles generally indicates an increase of the cell resistance at the lithium/solid electrolyte interface, i.e., partial loss of electrical contact between the lithium metal and the solid electrolyte or the formation of an electrically insulating SEI. By varying the applied current density, the critical current density can also be defined. Zhang et al. demonstrated the improved interfacial stability of the lithium/PEO solid electrolyte by adding Li<sub>0.33</sub>La<sub>0.557</sub>TiO<sub>3</sub> (LLTO) ceramic nanofiber into the PEO solid electrolyte.<sup>[96]</sup> The significantly lower polarization of the Li/(PEO/LLTO)/Li cells was measured ( $\pm 118$  mV) at 0.5 mA/cm<sup>2</sup> for 0.5 h per each cycle at room temperature compared to that of the Li/PEO/Li cell ( $\pm 415$  mV), and it sustains stable voltage over 1000 hours, indicating excellent electrochemical stability of the lithium/PEO-LLTO interface. The authors proposed that the improvement in the interfacial stability is attributed to the faster and more continuous ionic transport pathways of PEO-LLTO composite electrolytes. The symmetric cell experiment is also used to demonstrate the critical current density of these solid-state Li/S cells. Galvanostatic Li/solid electrolyte/Li symmetric cell tests with an increment of current density at each step can be performed to demonstrate the current density where the unstable voltage appears.

While electrochemical techniques provide comprehensive information about the ion and charge transport properties at the electrode/electrolyte interfaces, proper physical/chemical characterizations need to accompany and complement electrochemical observations to acquire in-depth understanding. Especially, ex situ and operando characterizations of the interfaces provide insights on the structural integrity, chemical reactions and ion diffusion which are needed to improve the cell performance and to identify a rational design principle for advanced solid-state Li/S cells. Here, we highlight several physicochemical characterization methods that were employed in reports on investigations of the solid electrolyte/sulfur electrode interfaces.

Scanning electron microscopy (SEM) of the planar and cross-sectional views of the electrode-electrolyte interface is the most widely used technique to study the structural robustness and interfacial contact between the electrode and electrolyte, which significantly affects the interfacial impedance. Furthermore, energy dispersive X-ray spectroscopy (EDX) enables examining the chemical composition profile and can provide elemental information about the solid electrolyte interphase. Wang et al. used SEM to give information on the fabrication process of 3D construction of the all-solid-state Li/Li<sub>2</sub>S cells built on a cathode material and the progression of the assembly. A cross-sectional view of the cell along with elemental mapping confirmed the formation of cathode-supported solid-state Li/S cell with a thin layer thickness of the solid electrolyte determined by area-specific presence of the elements.<sup>[97]</sup> Manthiram and coworkers performed ex-situ SEM/EDX analyses to image a cross-section of the LiSCION solid electrolyte in hybrid Li/LiPS cells after cycling. The line-scan profile of the sulfur elemental distribution inside the LiSCION membrane demonstrated that the sulfur species does not penetrate through the cell's solid membrane during electrochemical cycling.<sup>[123]</sup> In addition, the interfacial contact can also be examined by the direct imaging of the interface using SEM. Han et al. showed a cross-section view of the electrode-electrolyte interface and observed the enhancement of interfacial contact after the deposition of an Al<sub>2</sub>O<sub>3</sub> ultrathin layer on the garnet surface.<sup>[101]</sup>

Transmission electron microscopy (TEM) is typically used to investigate the morphology of granular cathode materials and cross-section of the solid electrolyte/cathode material interphases. Besides the direct imaging and electron energy loss spectroscopy (EELS) for elemental mapping, it is often employed along with the diffraction technique that can elucidate the sample's crystallinity and texture. Cui et al. used TEM to investigate the microstructure of LLZO@C cathode and revealed the porous structure of the cathode materials and the single crystallinity of the LLZO. Furthermore, high-resolution TEM combined with elemental mapping of various elements revealed the uniform distribution of Al and Nb dopants in the LLZO phase, which is critical for the stability and conductivity of cubic LLZO.<sup>[124]</sup>

In situ TEM is also extensively used to characterize lithium plating and stripping to reveal the change of physicochemical properties of the SEI layer during the charging/discharging. In particular, Yushin and coworkers observed in situ electron diffraction of the sulfur confined in carbon nanotube reactor, which was subsequently in contact with Li anode and Li<sub>2</sub>O electrolyte. During the lithiation, the TEM images and diffraction patterns were captured in real-time. The observed diffraction shows a transition from crystalline S<sub>8</sub> to a coexisting phase of crys-

talline Li<sub>2</sub>S and S<sub>8</sub>. After the completion of the electrochemical reaction, a homogeneous crystalline Li<sub>2</sub>S pattern was observed, suggesting that the sulfur undergoes direct conversion into Li<sub>2</sub>S without the formation of any other detectable intermediate phases.<sup>[125]</sup>

X-ray tomography is a nondestructive imaging technique to resolve the 3D structure inside the cell, and it is compatible with operando analysis. Shearing et al. reported in situ X-ray tomography of the S/C electrode and demonstrated the microstructural evolution of the cathode after multiple charge/discharge cycles. The 3D in operando technique observes the uneven distribution of the sulfur phase fraction within the cathode domain, suggesting significant mass transport limitations.<sup>[126]</sup>

Besides the direct visualization techniques, surface and chemical characteristics of the solid-state Li/S cells were examined by spectroscopic techniques such as nuclear magnetic resonance (NMR) spectroscopy and X-ray absorption spectroscopies. Yu et al.<sup>[127]</sup> reported lithium-ion exchange <sup>7</sup>Li NMR spectroscopy to access lithium-ion transport occurring at the interface between an argyrodite solid-electrolyte and a sulfide electrode. They performed two-dimensional exchange NMR spectroscopy (2D-EXSY) on a Li<sub>2</sub>S-Li<sub>6</sub>PS<sub>5</sub>Br cell at different stages in the preparation and before and after cycling. They observed that the lithium-ion kinetics over the interface dramatically decreased after cycling, most likely due to the poor interfacial contact caused by the large volumetric changes and increased diffusional energy barriers.<sup>[127]</sup> (Figure 5) X-ray absorption spectroscopy (XAS) is not only sensitive to the elements but also the local bonding chemistry and solvent environment, and thus, the reaction mechanism can be elucidated. Balsara et al. employed in situ XAS of Li/S cells with ether-based polymer electrolyte and investigated the intermediate polysulfides dissolved in oligomeric PEO. The first principle spectral simulation was used to interpret the experimental results indicating that the population distribution of polysulfide radical anions and short/long polysulfide dianions is strongly dependent on the state of charge.<sup>[128]</sup> Cui et al. measured sulfur K-edge X-ray absorption near-edge structure (XANES) for polymer electrolytes after cycling with and without encapsulated cathodes. The XANES analysis revealed the fingerprint peak of polysulfides only in the case of bare Li<sub>2</sub>S cathodes suggesting that the TiS<sub>2</sub> encapsulation trapped the polysulfides in the microstructure.<sup>[129]</sup>

### 3.1 | CCD

Works as an important index to compare the performances of Li metal anodes and indicates many intrinsic behaviors at high current densities in solid-state batteries.

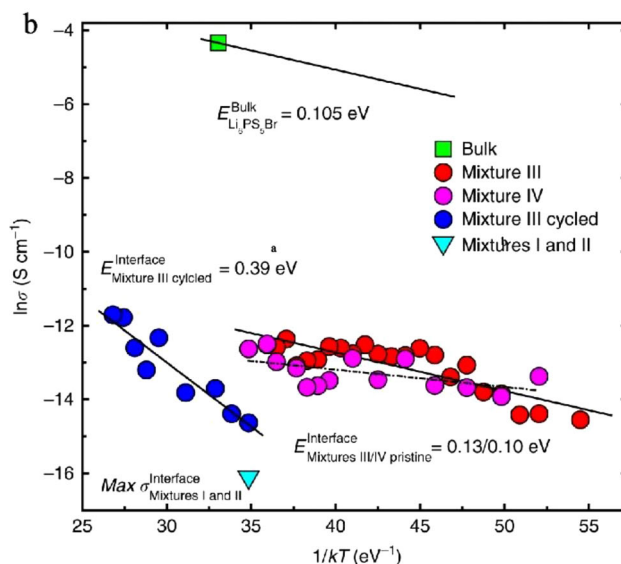
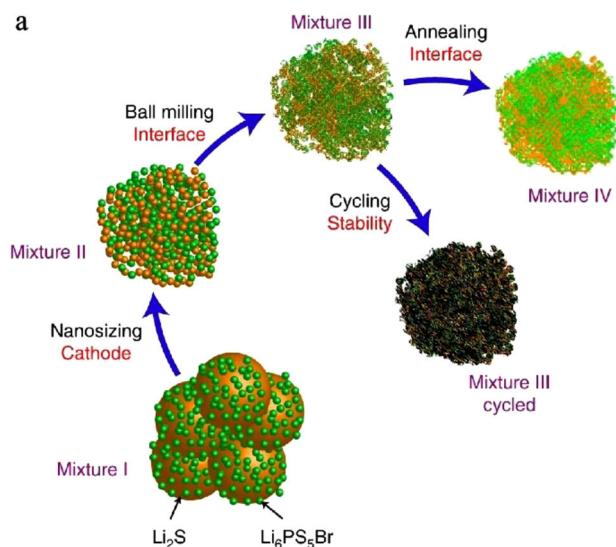


FIGURE 5 (a) Schematic representation of  $Li_2S$ - $Li_6PS_5Br$  cell at different stages. (b) Comparison of the lithium-ion conductivity for bulk  $Li_6PS_5Br$  and the conductivities of the  $Li_2S$ - $Li_6PS_5Br$  determined by NMR experiments (spin-lattice relaxation and 2D-EXSY, respectively).<sup>[127]</sup>

## 4 | SUMMARY AND OUTLOOK

Solid-state Li/S cells have recently attracted considerable attention for their improved safety and ability to remove the problematic Li-PS shuttle problem while preserving the great promise of conventional Li/S cells in achieving high specific energy storage solutions. Various solid superionic conductors, including polymer solid electrolytes and oxide-based and sulfide-based electrolytes, have dramatically improved the probability to realize solid-state Li/S cell technologies. While several other review papers discussing the progress in developing solid electrolyte materials are already available, this review introduces and summarizes the design and characterization strategies of interfaces between lithium and solid electrolyte, and sulfur and solid electrolyte in solid-state Li/S cells. We particularly categorize the approaches into two directions: (1) morphological design of electrode/solid electrolyte interface, (2) chemical interfacial design.

Forming a chemically-modified or microstructure-controlled electrode/electrolyte interface is essential to achieve promising electrochemical performances of solid-state Li/S cells. A defective and structurally unstable electrode-electrolyte interface leads to an insufficient electrochemical interface or lowering of the critical current density, resulting in interfacial failure of solid-state Li/S cells. In addition, the high chemical reactivity of lithium metal causes undesired decomposition of solid electrolytes at the interface, which may increase interfacial resistance.

The lithium/solid electrolyte interface of solid-state Li/S cells is identical to that of other lithium metal solid-state cells. Therefore, similar interfacial design strategies of the lithium metal solid-state cells can directly be adopted to

the solid-state Li/S cells. For stabilizing the lithium/solid electrolyte interface, forming an electrochemically stable and ionically conductive layer onto the lithium metal anode has shown its significant effect. Coating a thin layer of metal alloys, polymer electrolytes, or lithium halides at the electrode/electrolyte interface successfully improved the surface compatibility as well as regulated the uniform conduction of the ion currents. Surface polishing of the lithium metal anode is a helpful approach to form a stable initial lithium/solid electrolyte interface by reducing interfacial defects that cause current non-uniformity at the interface.

In contrast to the lithium-solid electrolyte interface, the physicochemical properties and electrochemical behavior of the sulfur electrode are distinct from those of oxide-based cathodes and major issues associated with the sulfur-solid electrolyte interface are: (1) the poor electronic and ionic conductivity of sulfur and  $Li_2S$  (2) slow Li-PS free, solid-state lithiation/delithiation process of sulfur (3) unstable interface due to the volumetric change of sulfur particles during lithiation and delithiation. Several research papers showed unique interfacial design concepts of sulfur-solid electrolyte incorporating 3D microstructure or forming homogeneous sulfur-carbon-solid electrolyte mixtures and demonstrated promising electrochemical performance of solid-state Li/S cells. However, interfacial electrochemistry of sulfur-solid electrolyte and their failure mechanisms have not been studied sufficiently.

Because of the unresolved technical difficulties discussed in this review, the current state-of-the-art of the solid-state Li/S cell is still far from commercialization. The cell performance is not comparable with that of

conventional Li/S cells using organic liquid electrolytes. The specific capacities of solid-state Li/S cells often relied on high testing temperatures, a small amount of liquid electrolyte, lower discharge cut-off voltage, low sulfur loading, and low sulfur content, or much lower test current density. Considering the promising physicochemical properties of solid superionic conductors, it is reasonable to regard that the unsatisfactory performance of solid-state Li/S cells results from the inappropriate interfacial design of the solid-state Li/S cells. In addition, solid-state Li/S cells will face almost the same challenges as the conventional Li/S cell, where high sulfur loading and low electrolyte to sulfur weight ratio are required while maintaining good sulfur utilization to achieve high specific energy under normal cell operation conditions. Enormous computational/experimental efforts in revealing and understanding the electrode-solid electrolyte interface are still strongly required, which should lead to a rational interfacial design that allows fast and sustainable electrochemical processes of solid-state Li/S cells. In addition, more advanced in-situ operando characterization methods commonly used in conventional Li/S cells can be implemented at the electrode/solid-electrolyte interface to fully understand the transport and reaction mechanism of the lithium-ions. Besides the technical difficulties, the process improvement is necessary by scaling up and integrating structured electrode and solid electrolyte manufacturing processes. Especially, high throughput, low-cost manufacturing can be expected by developing and optimizing roll-to-roll processes that can achieve seamless production of structured electrodes and thin solid electrolytes. Although the current state-of-the-art of solid-state Li/S cells is far from commercialization, intensive and continuous research effort dedicated to the interfacial analysis of solid-state Li/S cells can direct the development of practically viable Li/S cells in the future.

#### ACKNOWLEDGMENT

This work was supported by the 2021 Fulton Schools of Engineering Strategic Interest Seed Funding of Arizona State University.

#### AUTHOR CONTRIBUTIONS

The manuscript was written through the contributions of all authors. All authors have given approval to the final version of the manuscript.

#### CONFLICT OF INTEREST

The authors declare no conflict of interest.

#### DATA AVAILABILITY STATEMENT

This is a review paper, and no new data are included.

#### ORCID

Youngwoo Choo  <https://orcid.org/0000-0003-2715-0618>  
Yoon Hwa  <https://orcid.org/0000-0002-3622-4837>  
Elton J. Cairns  <https://orcid.org/0000-0002-1179-7591>

#### REFERENCES

1. T. T. Mai, P. Jadun, J. S. Logan, C. A. McMillan, M. Muratori, D. C. Steinberg, L. J. Vimmerstedt, B. Haley, R. Jones, B. Nelson, National Renewable Energy Lab.(NREL), Golden, CO (United States), **2018**.
2. K. Kelly, K. Bennion, E. Miller, B. Prohaska, National Renewable Energy Lab.(NREL), Golden, CO (United States), **2016**.
3. P. G. Bruce, S. A. Freunberger, L. J. Hardwick, J.-M. Tarascon, *Nat. Mater.* **2012**, *11*, 19–29.
4. J. B. Robinson, K. Xi, R. V. Kumar, A. C. Ferrari, H. Au, M.-M. Titirici, A. Parra-Puerto, A. Kucernak, S. D. S. Fitch, N. Garcia-Araez, Z. L. Brown, M. Pasta, L. Furness, A. J. Kibler, D. A. Walsh, L. R. Johnson, C. Holc, G. N. Newton, N. R. Champness, F. Markoulidis, C. Crean, R. C. T. Slade, E. I. Andritsos, Q. Cai, S. Babar, T. Zhang, C. Lekakou, N. Kulkarni, A. J. E. Rettie, R. Jervis, M. Cornish, M. Marinescu, G. Offer, Z. Li, L. Bird, C. P. Grey, M. Chhowalla, D. D. Lecce, R. E. Owen, T. S. Miller, D. J. L. Brett, S. Liatard, D. Ainsworth, P. R. Shearing, *J. Phys.: Energy* **2021**, *3*, 031501.
5. S. Ohno, W. G. Zeier, *Acc. Mater. Res.* **2021**, *2*, 869–880.
6. Y.-T. Liu, S. Liu, G.-R. Li, T.-Y. Yan, X.-P. Gao, *Advanced Science* **2020**, *7*, 1903693.
7. W. Wang, L. Huai, S. Wu, J. Shan, J. Zhu, Z. Liu, L. Yue, Y. Li, *ACS Nano* **2021**, *15*, 11619–11633.
8. Y. V. Mikhaylik, J. R. Akridge, *J. Electrochem. Soc.* **2004**, *151*, A1969.
9. B. Ding, J. Wang, Z. Fan, S. Chen, Q. Lin, X. Lu, H. Dou, A. Kumar Nanjundan, G. Yushin, X. Zhang, Y. Yamauchi, *Mater. Today* **2020**, *40*, 114–131.
10. X. Yang, J. Luo, X. Sun, *Chem. Soc. Rev.* **2020**, *49*, 2140–2195.
11. S. Hong, Y. Wang, N. Kim, S. B. Lee, *J. Mater. Sci.* **2021**, *56*, 8358–8382.
12. A. Manthiram, Y. Fu, S.-H. Chung, C. Zu, Y.-S. Su, *Chem. Rev.* **2014**, *114*, 11751–11787.
13. A. Manthiram, S.-H. Chung, C. Zu, *Adv. Mater.* **2015**, *27*, 1980–2006.
14. B. Tripathi, *Mater. Today: Proc.* **2021**, *42*, 1689–1691.
15. G. Li, Z. Li, B. Zhang, Z. Lin, *Front. Energy Res.* **2015**, *3*.
16. Y. Zheng, Y. Yao, J. Ou, M. Li, D. Luo, H. Dou, Z. Li, K. Amine, A. Yu, Z. Chen, *Chem. Soc. Rev.* **2020**, *49*, 8790–8839.
17. H. Hong, N. A. R. Che Mohamad, K. Chae, F. Marques Mota, D. H. Kim, *J. Mater. Chem. A* **2021**, *9*, 10012–10038.
18. D. Zhou, D. Shanmukaraj, A. Tkacheva, M. Armand, G. Wang, *Chemical* **2019**, *5*, 2326–2352.
19. D. Bresser, S. Passerini, B. Scrosati, *Chem. Commun.* **2013**, *49*, 10545–10562.
20. L. Wang, Y. Wang, Y. Xia, *Energy Environ. Sci.* **2015**, *8*, 1551–1558.
21. Y. Wang, G. Wang, P. He, J. Hu, J. Jiang, L.-Z. Fan, *Chem. Eng. J.* **2020**, *393*, 124705.
22. X. Yu, Z. Bi, F. Zhao, A. Manthiram, *Adv. Energy Mater.* **2016**, *6*, 1601392.
23. K. Fu, Y. Gong, G. T. Hitz, D. W. McOwen, Y. Li, S. Xu, Y. Wen, L. Zhang, C. Wang, G. Pastel, J. Dai, B. Liu, H. Xie, Y. Yao, E. D. Wachsman, L. Hu, *Energy Environ. Sci.* **2017**, *10*, 1568–1575.

24. K. Fu, Y. Gong, B. Liu, Y. Zhu, S. Xu, Y. Yao, W. Luo, C. Wang, S. D. Lacey, J. Dai, Y. Chen, Y. Mo, E. Wachsman, L. Hu, *Sci. Adv.* **2017**, *3*, e1601659.
25. M. Chen, C. Huang, Y. Li, S. Jiang, P. Zeng, G. Chen, H. Shu, H. Liu, Z. Li, X. Wang, *J. Mater. Chem. A* **2019**, *7*, 10293–10302.
26. J. B. Goodenough, H. Y. P. Hong, J. A. Kafalas, *Mater. Res. Bull.* **1976**, *11*, 203–220.
27. J. S. Thokchom, B. Kumar, *J. Power Sources* **2010**, *195*, 2870–2876.
28. T. Thompson, S. Yu, L. Williams, R. D. Schmidt, R. Garcia-Mendez, J. Wolfenstine, J. L. Allen, E. Kioupakis, D. J. Siegel, J. Sakamoto, *ACS Energy Lett.* **2017**, *2*, 462–468.
29. M. Amores, H. El-Shinawi, I. McClelland, S. R. Yeandel, P. J. Baker, R. I. Smith, H. Y. Playford, P. Goddard, S. A. Corr, E. J. Cussen, *Nat. Commun.* **2020**, *11*, 6392.
30. A. Hayashi, A. Sakuda, M. Tatsumisago, *Front. Energy Res.* **2016**, *4*.
31. Y. Kato, S. Hori, T. Saito, K. Suzuki, M. Hirayama, A. Mitsui, M. Yonemura, H. Iba, R. Kanno, *Nat. Energy* **2016**, *1*, 16030.
32. N. Kamaya, K. Homma, Y. Yamakawa, M. Hirayama, R. Kanno, M. Yonemura, T. Kamiyama, Y. Kato, S. Hama, K. Kawamoto, A. Mitsui, *Nat. Mater.* **2011**, *10*, 682–686.
33. A. Hayashi, T. Ohtomo, F. Mizuno, K. Tadanaga, M. Tatsumisago, *Electrochem. Commun.* **2003**, *5*, 701–705.
34. J. Lau, R. H. DeBlock, D. M. Butts, D. S. Ashby, C. S. Choi, B. S. Dunn, *Adv. Energy Mater.* **2018**, *8*, 1800933.
35. Y. Shan, L. Li, X. Yang, *ACS Appl. Energy Mater.* **2021**, *4*, 5101–5112.
36. Y. Zhao, Y. Zhang, D. Gosselink, T. N. L. Doan, M. Sadhu, H.-J. Cheang, P. Chen, *Membranes* **2012**, *2*, 553–564.
37. X. Judez, H. Zhang, C. Li, J. A. González-Marcos, Z. Zhou, M. Armand, L. M. Rodríguez-Martinez, *J. Phys. Chem. Lett.* **2017**, *8*, 1956–1960.
38. G. G. Eshetu, X. Judez, C. Li, M. Martínez-Ibañez, I. Gracia, O. Bondarchuk, J. Carrasco, L. M. Rodríguez-Martinez, H. Zhang, M. Armand, *J. Am. Chem. Soc.* **2018**, *140*, 9921–9933.
39. H. Zhang, U. Oteo, X. Judez, G. G. Eshetu, M. Martínez-Ibañez, J. Carrasco, C. Li, M. Armand, *Joule* **2019**, *3*, 1689–1702.
40. X. Judez, H. Zhang, C. Li, G. G. Eshetu, J. A. González-Marcos, M. Armand, L. M. Rodríguez-Martinez, *J. Electrochem. Soc.* **2017**, *165*, A6008–A6016.
41. J. R. Nair, L. Imholt, G. Bruncklaus, M. Winter, *Electrochem. Soc. Interface* **2019**, *28*, 55–61.
42. O. Borodin, G. D. Smith, *Macromolecules* **2006**, *39*, 1620–1629.
43. H. Wang, L. Sheng, G. Yasin, L. Wang, H. Xu, X. He, *Energy Storage Mater.* **2020**, *33*, 188–215.
44. Y. Zhao, L. Wang, Y. Zhou, Z. Liang, N. Tavajohi, B. Li, T. Li, *Advanced Science* **2021**, *8*, 2003675.
45. M. Liu, D. Zhou, Y.-B. He, Y. Fu, X. Qin, C. Miao, H. Du, B. Li, Q.-H. Yang, Z. Lin, T. S. Zhao, F. Kang, *Nano Energy* **2016**, *22*, 278–289.
46. Y. Xiao, Y. Wang, S.-H. Bo, J. C. Kim, L. J. Miara, G. Ceder, *Nat. Rev. Mater.* **2020**, *5*, 105–126.
47. F. Zheng, M. Kotobuki, S. Song, M. O. Lai, L. Lu, *J. Power Sources* **2018**, *389*, 198–213.
48. Z. Ding, J. Li, J. Li, C. An, *J. Electrochem. Soc.* **2020**, *167*, 070541.
49. T. Krauskopf, F. H. Richter, W. G. Zeier, J. Janek, *Chem. Rev.* **2020**, *120*, 7745–7794.
50. K. J. Kim, M. Balaish, M. Wadaguchi, L. Kong, J. L. M. Rupp, *Adv. Energy Mater.* **2021**, *11*, 2002689.
51. J. Kasemchainan, S. Zekoll, D. Spencer Jolly, Z. Ning, G. O. Hartley, J. Marrow, P. G. Bruce, *Nat. Mater.* **2019**, *18*, 1105–1111.
52. C. Yu, S. Ganapathy, N. J. J. de Klerk, I. Roslon, E. R. H. van Eck, A. P. M. Kentgens, M. Wagemaker, *J. Am. Chem. Soc.* **2016**, *138*, 11192–11201.
53. R. Elazari, G. Salitra, Y. Talyosef, J. Grinblat, C. Scordilis-Kelley, A. Xiao, J. Affinito, D. Aurbach, *J. Electrochem. Soc.* **2010**, *157*, A1131.
54. A. Banerjee, X. Wang, C. Fang, E. A. Wu, Y. S. Meng, *Chem. Rev.* **2020**, *120*, 6878–6933.
55. Z. Yu, Y. Cui, Z. Bao, *Cell Rep. Phys. Sci.* **2020**, *1*, 100119.
56. D. Lei, K. Shi, H. Ye, Z. Wan, Y. Wang, L. Shen, B. Li, Q.-H. Yang, F. Kang, Y.-B. He, *Adv. Funct. Mater.* **2018**, *28*, 1707570.
57. H. Pan, Z. Cheng, P. He, H. Zhou, *Energy Fuels* **2020**, *34*, 11942–11961.
58. E. Umeshbabu, B. Zheng, Y. Yang, *Electrochem. Energy Rev.* **2019**, *2*, 199–230.
59. H. Wang, X. Cao, W. Liu, X. Sun, *Front. Energy Res.* **2019**, *7*.
60. Y. Wang, E. Sahadeo, G. Rubloff, C.-F. Lin, S. B. Lee, *J. Mater. Sci.* **2019**, *54*, 3671–3693.
61. X. Yu, A. Manthiram, *Acc. Chem. Res.* **2017**, *50*, 2653–2660.
62. W. Xu, J. Wang, F. Ding, X. Chen, E. Nasybulin, Y. Zhang, J.-G. Zhang, *Energy Environ. Sci.* **2014**, *7*, 513–537.
63. H. Liu, X.-B. Cheng, R. Xu, X.-Q. Zhang, C. Yan, J.-Q. Huang, Q. Zhang, *Adv. Energy Mater.* **2019**, *9*, 1902254.
64. L. Gireaud, S. Grugeon, S. Laruelle, B. Yrieix, J. M. Tarascon, *Electrochem. Commun.* **2006**, *8*, 1639–1649.
65. L. Porz, T. Swamy, B. W. Sheldon, D. Rettenwander, T. Frömling, H. L. Thaman, S. Berendts, R. Uecker, W. C. Carter, Y.-M. Chiang, *Adv. Energy Mater.* **2017**, *7*, 1701003.
66. Q. Tu, L. Barroso-Luque, T. Shi, G. Ceder, *Cell Rep. Phys. Sci.* **2020**, *1*, 100106.
67. S. Wang, J. Wang, J. Liu, H. Song, Y. Liu, P. Wang, P. He, J. Xu, H. Zhou, *J. Mater. Chem. A* **2018**, *6*, 21248–21254.
68. H. Huo, J. Luo, V. Thangadurai, X. Guo, C.-W. Nan, X. Sun, *ACS Energy Lett.* **2020**, *5*, 252–262.
69. X. Fu, T. Wang, W. Shen, M. Jiang, Y. Wang, Q. Dai, D. Wang, Z. Qiu, Y. Zhang, K. Deng, Q. Zeng, N. Zhao, X. Guo, Z. Liu, J. Liu, Z. Peng, *Adv. Mater.* **2020**, *32*, 2000575.
70. A. Sharafi, E. Kazyak, A. L. Davis, S. Yu, T. Thompson, D. J. Siegel, N. P. Dasgupta, J. Sakamoto, *Chem. Mater.* **2017**, *29*, 7961–7968.
71. S. Hao, H. Zhang, W. Yao, J. Lin, *J. Power Sources* **2018**, *393*, 128–134.
72. Y. Li, B. Xu, H. Xu, H. Duan, X. Lü, S. Xin, W. Zhou, L. Xue, G. Fu, A. Manthiram, J. B. Goodenough, *Angew. Chem. Int. Ed.* **2017**, *56*, 753–756.
73. L. Cheng, W. Chen, M. Kunz, K. Persson, N. Tamura, G. Chen, M. Doeff, *ACS Appl. Mater. Interfaces* **2015**, *7*, 2073–2081.
74. L. Cheng, J. S. Park, H. Hou, V. Zorba, G. Chen, T. Richardson, J. Cabana, R. Russo, M. Doeff, *J. Mater. Chem. A* **2014**, *2*, 172–181.
75. Y. Gu, W.-W. Wang, J.-W. He, S. Tang, H.-Y. Xu, J.-W. Yan, Q.-H. Wu, X.-B. Lian, M.-S. Zheng, Q.-F. Dong, B.-W. Mao, *Chem. ElectroChem.* **2019**, *6*, 181–188.

76. Y. Gu, W.-W. Wang, Y.-J. Li, Q.-H. Wu, S. Tang, J.-W. Yan, M.-S. Zheng, D.-Y. Wu, C.-H. Fan, W.-Q. Hu, Z.-B. Chen, Y. Fang, Q.-H. Zhang, Q.-F. Dong, B.-W. Mao, *Nat. Commun.* **2018**, *9*, 1339.
77. A. Sharafi, S. Yu, M. Naguib, M. Lee, C. Ma, H. M. Meyer, J. Nanda, M. Chi, D. J. Siegel, J. Sakamoto, *J. Mater. Chem. A* **2017**, *5*, 13475–13487.
78. L. Chen, W. Li, L.-Z. Fan, C.-W. Nan, Q. Zhang, *Adv. Funct. Mater.* **2019**, *29*, 1901047.
79. S. Xu, D. W. McOwen, C. Wang, L. Zhang, W. Luo, C. Chen, Y. Li, Y. Gong, J. Dai, Y. Kuang, C. Yang, T. R. Hamann, E. D. Wachsman, L. Hu, *Nano Lett.* **2018**, *18*, 3926–3933.
80. Y. Liu, D. Lin, Y. Jin, K. Liu, X. Tao, Q. Zhang, X. Zhang, Y. Cui, *Sci. Adv.* **2017**, *3*, ea00713.
81. G. T. Hitz, D. W. McOwen, L. Zhang, Z. Ma, Z. Fu, Y. Wen, Y. Gong, J. Dai, T. R. Hamann, L. Hu, E. D. Wachsman, *Mater. Today* **2019**, *22*, 50–57.
82. A. Unemoto, S. Yasaku, G. Nogami, M. Tazawa, M. Taniguchi, M. Matsuo, T. Ikeshoji, S.-I. Orimo, *Appl. Phys. Lett.* **2014**, *105*, 083901.
83. M. Agostini, Y. Aihara, T. Yamada, B. Scrosati, J. Hassoun, *Solid State Ion.* **2013**, *244*, 48–51.
84. E. Umeshbabu, B. Zheng, J. Zhu, H. Wang, Y. Li, Y. Yang, *ACS Appl. Mater. Interfaces* **2019**, *11*, 18436–18447.
85. X. Yao, N. Huang, F. Han, Q. Zhang, H. Wan, J. P. Muzerwa, C. Wang, X. Xu, *Adv. Energy Mater.* **2017**, *7*, 1602923.
86. S. Das, P. Ngene, P. Norby, T. Vegge, P. E. de Jongh, D. Blanchard, *J. Electrochem. Soc.* **2016**, *163*, A2029–A2034.
87. R.-c. Xu, X.-h. Xia, X.-l. Wang, Y. Xia, J.-p. Tu, *J. Mater. Chem. A* **2017**, *5*, 2829–2834.
88. M. Nagao, A. Hayashi, M. Tatsumisago, *Electrochimica Acta* **2011**, *56*, 6055–6059.
89. M. Nagao, A. Hayashi, M. Tatsumisago, *J. Mater. Chem.* **2012**, *22*, 10015–10020.
90. M. Chen, S. Adams, *J. Solid State Electrochem.* **2015**, *19*, 697–702.
91. J. Yi, L. Chen, Y. Liu, H. Geng, L.-Z. Fan, *ACS Appl. Mater. Interfaces* **2019**, *11*, 36774–36781.
92. C. Zheng, K. Wang, L. Li, H. Huang, C. Liang, Y. Gan, X. He, W. Zhang, J. Zhang, *Front. Energy Res.* **2021**, *8*.
93. Y. Yang, G. Zheng, S. Misra, J. Nelson, M. F. Toney, Y. Cui, *J. Am. Chem. Soc.* **2012**, *134*, 15387–15394.
94. K. Cai, M.-K. Song, E. J. Cairns, Y. Zhang, *Nano Lett.* **2012**, *12*, 6474–6479.
95. Z. Lin, Z. Liu, N. J. Dudney, C. Liang, *ACS Nano* **2013**, *7*, 2829–2833.
96. P. Zhu, C. Yan, J. Zhu, J. Zang, Y. Li, H. Jia, X. Dong, Z. Du, C. Zhang, N. Wu, M. Dirican, X. Zhang, *Energy Storage Mater.* **2019**, *17*, 220–225.
97. R. Xu, J. Yue, S. Liu, J. Tu, F. Han, P. Liu, C. Wang, *ACS Energy Lett.* **2019**, *4*, 1073–1079.
98. S. Xu, D. W. McOwen, L. Zhang, G. T. Hitz, C. Wang, Z. Ma, C. Chen, W. Luo, J. Dai, Y. Kuang, E. M. Hitz, K. Fu, Y. Gong, E. D. Wachsman, L. Hu, *Energy Storage Mater.* **2018**, *15*, 458–464.
99. K. B. Hatzell, X. C. Chen, C. L. Cobb, N. P. Dasgupta, M. B. Dixit, L. E. Marbella, M. T. McDowell, P. P. Mukherjee, A. Verma, V. Viswanathan, A. S. Westover, W. G. Zeier, *ACS Energy Lett.* **2020**, *5*, 922–934.
100. W. Li, Q. Wang, J. Jin, Y. Li, M. Wu, Z. Wen, *Energy Storage Mater.* **2019**, *23*, 299–305.
101. X. Han, Y. Gong, K. Fu, X. He, G. T. Hitz, J. Dai, A. Pearse, B. Liu, H. Wang, G. Rubloff, Y. Mo, V. Thangadurai, E. D. Wachsman, L. Hu, *Nat. Mater.* **2017**, *16*, 572–579.
102. S. Chen, J. Zhang, L. Nie, X. Hu, Y. Huang, Y. Yu, W. Liu, *Adv. Mater.* **2021**, *33*, 2002325.
103. C.-L. Tsai, V. Roddatis, C. V. Chandran, Q. Ma, S. Uhlenbruck, M. Bram, P. Heitjans, O. Guillon, *ACS Appl. Mater. Interfaces* **2016**, *8*, 10617–10626.
104. S. Wei, L. Ma, K. E. Hendrickson, Z. Tu, L. A. Archer, *J. Am. Chem. Soc.* **2015**, *137*, 12143–12152.
105. J. Liu, T. Qian, M. Wang, J. Zhou, N. Xu, C. Yan, *Nano Lett.* **2018**, *18*, 4598–4605.
106. X. Fan, X. Ji, F. Han, J. Yue, J. Chen, L. Chen, T. Deng, J. Jiang, C. Wang, *Sci. Adv.* **2018**, *4*, eaau9245.
107. T. Chen, W. Kong, P. Zhao, H. Lin, Y. Hu, R. Chen, W. Yan, Z. Jin, *Chem. Mater.* **2019**, *31*, 7565–7573.
108. T. Deng, X. Ji, Y. Zhao, L. Cao, S. Li, S. Hwang, C. Luo, P. Wang, H. Jia, X. Fan, X. Lu, D. Su, X. Sun, C. Wang, J.-G. Zhang, *Adv. Mater.* **2020**, *32*, 2000030.
109. X. Yu, A. Manthiram, *Adv. Funct. Mater.* **2019**, *29*, 1805996.
110. B. Sun, K. Liu, J. Lang, M. Fang, Y. Jin, H. Wu, *Electrochimic. Acta* **2018**, *284*, 662–668.
111. A. M. Tripathi, W.-N. Su, B. J. Hwang, *Chem. Soc. Rev.* **2018**, *47*, 736–851.
112. R. S. Nicholson, *Anal. Chem.* **1965**, *37*, 1351–1355.
113. Y. Xia, Y. F. Liang, D. Xie, X. L. Wang, S. Z. Zhang, X. H. Xia, C. D. Gu, J. P. Tu, *Chem. Eng. J.* **2019**, *358*, 1047–1053.
114. D. Cai, D. Wang, Y. Chen, S. Zhang, X. Wang, X. Xia, J. Tu, *Chem. Eng. J.* **2020**, *394*, 124993.
115. M. Watanabe, K. Sanui, N. Ogata, T. Kobayashi, Z. Ohtaki, *J. Appl. Phys.* **1985**, *57*, 123–128.
116. S. Chandra, S. K. Tolpadi, S. A. Hashmi, *Solid State Ionics* **1988**, *28-30*, 651–655.
117. J. B. Wagner, C. Wagner, *J. Chem. Phys.* **1957**, *26*, 1597–1601.
118. R. C. AGRAWAL, *Indian j. pure appl. Phys.* **1999**, *37*, 294–301.
119. P. G. Bruce, J. Evans, C. A. Vincent, *Solid State Ionics* **1988**, *28-30*, 918–922.
120. P. G. Bruce, C. A. Vincent, *J. Electroanal. Chem. Interf. Electrochem.* **1987**, *225*, 1–17.
121. C. Zhou, S. Bag, T. He, B. Lv, V. Thangadurai, *Appl. Mater. Today* **2020**, *19*, 100585.
122. R. Elizalde-Segovia, A. Irshad, B. Zayat, S. R. Narayanan, *J. Electrochem. Soc.* **2020**, *167*, 140529.
123. X. Yu, Z. Bi, F. Zhao, A. Manthiram, *ACS Appl. Mater. Interfaces* **2015**, *7*, 16625–16631.
124. X. Tao, Y. Liu, W. Liu, G. Zhou, J. Zhao, D. Lin, C. Zu, O. Sheng, W. Zhang, H.-W. Lee, Y. Cui, *Nano Lett.* **2017**, *17*, 2967–2972.
125. H. Kim, J. T. Lee, A. Magasinski, K. Zhao, Y. Liu, G. Yushin, *Adv. Energy Mater.* **2015**, *5*, 1501306.
126. A. Yermukhambetova, C. Tan, S. R. Daemi, Z. Bakenov, J. A. Darr, D. J. L. Brett, P. R. Shearing, *Sci. Rep.* **2016**, *6*, 35291.
127. C. Yu, S. Ganapathy, E. R. H. v Eck, H. Wang, S. Basak, Z. Li, M. Wagemaker, *Nat. Commun.* **2017**, *8*, 1086.
128. K. H. Wujcik, T. A. Pascal, C. D. Pemmaraju, D. Devaux, W. C. Stolte, N. P. Balsara, D. Prendergast, *Adv. Energy Mater.* **2015**, *5*, 1500285.
129. X. Gao, X. Zheng, J. Wang, Z. Zhang, X. Xiao, J. Wan, Y. Ye, L.-Y. Chou, H. K. Lee, J. Wang, R. A. Vilá, Y. Yang, P. Zhang, L.-W. Wang, Y. Cui, *Nano Lett.* **2020**, *20*, 5496–5503.

## AUTHOR BIOGRAPHIES



Dr. Youngwoo Choo is a 2022 Chancellor's Postdoctoral Research Fellow at the University of Technology Sydney (UTS), Australia. He received his BS and MS in Chemical and Biological Engineering from the

Seoul National University and received his PhD degree in Chemical and Environmental Engineering from Yale University in 2019. Before joining UTS, he was a Postdoctoral Fellow at the Lawrence Berkeley National Laboratory and studied acetal-based polymer electrolytes. His research interest is centered on engineered nanostructures, ion transport properties in polymer electrolytes, and their characterizations.



Dr. Yoon Hwa is an assistant professor at Arizona State University in the U.S. He received his Ph.D. in Material Science from Seoul National University (South Korea) in 2013 and worked at the University of California Berkeley and Lawrence Berkeley National Laboratory (USA) as a postdoc and

research scientist in 2014–2020. Throughout his career, his research effort has mainly been dedicated to the field of advanced rechargeable batteries and laser additive manufacturing technologies. His research focuses on developing advanced energy storage materials or rational 3D architectures of rechargeable battery electrodes using advanced manufacturing technologies.



**Elton J. Cairns, University of California, and Lawrence Berkeley National Laboratory, Berkeley, CA 94720**, Professor of the Graduate School, UC Berkeley; Faculty Senior Scientist, LBNL; BS Chemistry, BS Chem.Eng'g, Michigan Technological Univer-

sity; Ph.D. Chem. Eng'g, Univ. of California, Berkeley; Assoc. Lab Director, Lawrence Berkeley National Lab, 1978–96, Honorary Member, International Society of Electrochemistry, Melvin Calvin Medal of Distinction, Michigan Technological University; Fellow, Electrochemical Society; Fellow, International Society of Electrochemistry; Fellow, American Institute of Chemists; Honorary Member, International Society of Electrochemistry; IR-100 Awards (1967, 1992); International Society of Electrochemistry (President, 1999–2000); The Electrochemical Society (President, 1989–90); Editor, *Electrochimica Acta* (1987–2004); Division Editor, *Journal of The Electrochemical Society* 1973–1990; More than 300 publications, 25 patents, book on fuel cells. Research interests: Li cells, fuel cells, electrocatalysis, electrochemistry.

**How to cite this article:** Y. Choo, Y. Hwa, E. J. Cairns. *Electrochem Sci Adv.* **2022**, *2*, e2100154.  
<https://doi.org/10.1002/elsa.202100154>